



**SCHOOL OF MECHANICAL, INDUSTRIAL &
AERONAUTICAL ENGINEERING
UNIVERSITY OF THE WITWATERSRAND,
JOHANNESBURG**

MECN4029: MECHATRONICS II

**MECHATRONIC SYSTEMS DESIGN: AGGRESSIVE
MANEUVER STABILIZATION FOR A MINIDRONE**

Students

Osca Kholopha (1863498)
Sandiswa Nkabinde (2324218)
Thobela Mzaca (1844385)
Romeo Raleting (1419355)

Supervisor

Dr A Panday

Mechatronic group assignment submitted to the Faculty of Engineering and the Built Environment,
University of the Witwatersrand, Johannesburg, in partial fulfilment of the requirements
for the degree of Bachelor of Science in Engineering.

Johannesburg, 22 May 2025



Disclosure – Use of Artificial-Intelligence (AI) Generated Content

2025 V1.0

Students must acknowledge all use of AI.

Select all applicable statements and complete the sections fully. **Delete all statements that are not applicable.**

1. Disclosure: No AI use

I acknowledge that no AI tools/technologies (Grammarly, ChatGPT, Bard, Quillbot, OpenAI etc) were used in the completion of this assessment.

2. Disclosure: Editing/refining grammar, spelling, formatting

I acknowledge the use of Chat GPT, 4.0 mini, Gemini, DeepSeek, May 2025(<https://chatgpt.com/><https://gemini.google.com/><https://chat.deepseek.com/>) to improve the explain what was edited/refined. I uploaded the text for my MECN4029A Mechatronics II Assignment, and I entered the following prompts on 19-22,May,2025:

Original prompt: "Correct any grammatical error and punctuations in the following passage. Help me set up the document settings in Latex"

Follow-up prompt: "Make it coherent and cohesive"

The output from these prompts was used to. A well structured paragraph with corrected grammar and punctuations. Latex code structure for reporting.

3. Disclosure: Generated/manipulated text – list each occurrence

I acknowledge the use of XYZ, version, Month, Year (web url) to explain what you used AI for. I entered the following prompt on Date, Month, Year:

"Paste the prompt"

The output from these prompts was used as update old text with grammar and spelling error and provide a better narrative flow.

4. Disclosure: Generated/manipulated image – list each occurrence

I acknowledge the use of XYZ, version, Month, Year (web url) to explain what you used AI for. I entered the following prompt on Date, Month, Year:

"Paste the prompt"

The output from these prompts was used as explain what the image was used for.

5. Disclosure: Generated/manipulated code – list each occurrence

School of Mechanical, Industrial & Aeronautical Engineering, 1st Floor, South West Engineering Building, Braamfontein Campus East
Private Bag 3, WITS, 2050 T +27 11 717 7308 | www.wits.ac.za/mecheng



I acknowledge the use of XYZ, version, Month, Year (web url) to explain what you used AI for. I entered the following prompt on Date, Month, Year:

"I help me identify any syntax error in my code"

The output from these prompts was used as An error less code with corrected syntax.

I declare that the disclosure is complete and truthful.

Student number: 1419355; 1863498; 2324218; 1844385

Course code: MECN4029A

Date: 22/May/2025

Contents

1 Introduction	1
1.1 Background	1
1.2 Drone Scenarios for Inspection	1
1.2.1 Hovering from a Freehand Throw	1
1.2.2 Hovering from a Free Fall	1
1.2.3 Hovering from an Upside-Down Orientation	2
1.2.4 Maintaining Hover with Aggressive Inputs	2
1.2.5 Emergency Response within a Specific Timeframe	2
2 Literature Review	3
2.1 QuadrotorDrone components and system	3
2.2 Quadrotor Model Assumptions	3
2.3 Quadrotor System Modeling	3
2.4 Design Objectives	4
2.5 Problem Statement	5
3 Performance Specifications	6
3.1 Time-domain Performance Specifications	6
3.2 Frequency-domain Performance Specifications	6
4 Mathematical Model	8
4.1 Quadrotor Model Assumptions	8
4.1.1 Structural Assumptions	8
4.1.2 Aerodynamic Assumptions	8
4.1.3 Control and Measurement Assumptions	8
4.2 Mathematical Model	9
4.2.1 Reference Frames and Coordinate Transformations	9
4.2.2 Forces and Moments Analysis	9
4.3 Nonlinear Dynamics	10
4.3.1 Translational Dynamics	10
4.3.2 Rotational Dynamics	11
4.3.3 Control Inputs	11
4.4 Linear Model	12
4.4.1 Translational Dynamics	12
4.4.2 Roll	13
4.4.3 Pitch	14
4.4.4 Yaw	14
4.5 Equations of Motions for the System in Time-Domain and Frequency Domain	16
4.5.1 Transfer Functions of the System	16
4.5.2 Elevation	16
4.5.3 Roll	16
4.5.4 Pitch	17
4.5.5 Yaw	17
4.6 State-Space Representation of Quadrotor Dynamics	18
4.6.1 System Matrix (A)	18
5 System Response Analysis	21

5.1 Non-linear Plant	21
5.1.1 Non-linear Time-response of the System	21
5.2 System Response Analysis	22
5.2.1 Linear Plant	22
5.2.2 Linear Time Response of the System to the Impulse Input	22
5.2.3 Linear time response of the system to the step input	23
5.2.4 Comparison of non-linear and linear uncontrolled models	23
5.3 Linear model stability behaviour	24
5.3.1 Zero-Pole Stability Analysis	24
5.4 Nyquist Stability Criterion	26
5.4.1 Routh-Hurwitz Stability Criterion	28
5.4.2 Bode Plot Analysis	28
6 Controller Design	30
6.1 PID controller	30
6.1.1 Different controller designs	30
6.1.2 PID tuning	37
6.2 Rationale for Quadrotor Implementation	37
6.2.1 System Setup	38
6.2.2 Desired Characteristic Equation	38
6.2.3 Controller Structure	38
6.2.4 Closed-Loop Analysis	38
6.2.5 Closed-loop characteristic equation	38
6.2.6 Gain Calculation	39
6.2.7 Final PID Gains	39
6.2.8 PID controller evaluation	41
6.3 Root-locus technique	42
6.3.1 Concept	42
6.3.2 Controller Design Methodology	42
6.3.3 Root locus solution	43
6.3.4 PID Control Using Routh-Hurwitz	48
6.3.5 Less Dominant Root Concept	51
7 Discussion	53
8 Conclusion	54

List of Figures

1	UAV in operation for building inspection	1
2	Labelled Quadrotor drone components	3
3	Insert Caption	9
4	Drone Top view	10
5	Quadrotor axis and parameters	12
6	Overall Plant Block Diagram	19
7	Linear Model Block Diagram	20
8	Linear Block diagram s-domain	20
9	System non-linear response	21
10	Impulse Input linear response	22
11	Step response of the linear system	23
12	Pole Zero plots for quadrotor: (a) Roll, (b) Pitch, (c) Yaw, and (d) Elevation.	25
13	Nyquist plots for quadrotor dynamics: (a) Roll, (b) Pitch, (c) Yaw, and (d) Elevation.	27
14	Bode plots for quadrotor dynamics: (a) Roll, (b) Pitch, (c) Yaw, and (d) Elevation.	29
15	System Controller	30
16	PD Freehand throw control	33
17	PD Free fall control	34
18	PD Upside down control	34
19	PID Freehand throw control	36
20	PID Free Fall control	36
21	PID Upside down control	37
22	Tuned PID response	40
23	Non linear Free hand throw PID controller output	41
24	Non linear Free fall PID controller output	41
25	Non linear Upside down PID controller output	42
26	Root locus plots of the integral control of the altitude controller.	44
27	Root locus plots of the integral control of the pitch and/or roll controller.	44
28	Root locus plots of the integral control of the yaw attitude controller.	45
29	Root locus plot of proportional derivative controller applied for the altitude controller	46
30	Root locus plot of proportional derivative controller applied for Roll/Pitch	47
31	Root locus Integral control for yaw	48
32	PID control root locus for altitude	49
33	PID for Roll/Pitch	50
34	PID controller root locus for the yaw controller.	51

List of Tables

1	Time-domain performance specifications	6
2	Quadrotor Model Specifications	7
3	Equations of Motions for the System in Time-Domain and Frequency Domain	16
4	System Parameters	17
5	Transfer function for elevation, roll, pitch, and yaw	24
6	Input values of frequencies to estimate the shape of Nyquist plot	26
7	Routh-Hurwitz stability table	28
8	Bode functions from Transfer Function	29
9	Controller Gains for Various Third Pole Locations	39
10	Final Summary Table of PID Gains (Analytical)	39
11	PD Control Varies Proportional Control in K	48
12	Root Locus Points for PID Altitude Control ($k_p = 5.28, k_I = 4.65, k_D = 3.4$)	50
13	Yaw/Roll Controller with PID Gains ($k_p = 0.000546, k_I = 0.000848, k_D = 0.00747$)	51
14	Yaw Controller Root Locus with PID Gains ($k_p = 0.000411, k_I = 0.000639, k_D = 0.00563$)	51
15	Minimum Time Constant for Different Controllers	52
16	Breakaway Points and Minimum Time Constants	52

Nomenclature

Symbol	Description	Units
m	Mass of the quadrotor	kg
g	Acceleration due to gravity	m/s^2
I_{xx}, I_{yy}, I_{zz}	Moments of inertia	$\text{kg}\cdot\text{m}^2$
J_{TP}	Rotor inertia	$\text{kg}\cdot\text{m}^2$
ω_i	Angular velocity of rotor i	rad/s
ω_0	Nominal rotor speed	rad/s
k	Thrust coefficient	$\text{N}\cdot\text{s}^2/\text{rad}^2$
d	Drag coefficient	$\text{N}\cdot\text{m}\cdot\text{s}^2/\text{rad}^2$
l	Rotor arm length	m
U_1	Total thrust input	N
U_2	Roll torque input	$\text{N}\cdot\text{m}$
U_3	Pitch torque input	$\text{N}\cdot\text{m}$
U_4	Yaw torque input	$\text{N}\cdot\text{m}$
x, y, z	Position in inertial frame	m
ϕ	Roll angle	rad
θ	Pitch angle	rad
ψ	Yaw angle	rad
\dot{x}	Velocity in x -direction	m/s
\ddot{x}	Acceleration in x -direction	m/s^2
$X(s)$	Laplace transform of $x(t)$	-
F_i	Thrust from rotor i	N
τ_i	Torque from rotor i	$\text{N}\cdot\text{m}$
F_T	Total thrust	N
M_x	Moment about x -axis	$\text{N}\cdot\text{m}$
M_y	Moment about y -axis	$\text{N}\cdot\text{m}$
M_z	Moment about z -axis	$\text{N}\cdot\text{m}$
\mathbf{R}	Rotation matrix	-
\mathbf{x}	State vector	-
\mathbf{u}	Control input vector	-
Δ	Small perturbation	-

Notation	Meaning
W	Inertial (world) frame
B	Body-fixed frame
$(\cdot)_0$	Equilibrium condition
$(\cdot)_i$	Quantity for rotor i
$(\cdot)_{xx}$	Component along x -axis
$(\cdot)^T$	Matrix transpose
$(\cdot)^{-1}$	Matrix inverse

1 Introduction

1.1 Background

High-rise buildings are important to modern urban landscapes, but their maintenance and inspection present significant challenges. Traditional methods often require inspectors to work at extreme heights using scaffolding, cranes, or rappelling equipment, which can be slow, expensive, and hazardous. These approaches also disrupt building operations and may not provide comprehensive coverage due to accessibility limitations. Drones, or unmanned aerial vehicles (UAVs), offer a transformative solution by enabling rapid, non-invasive inspections without putting human workers at risk. Their ability to access difficult-to-reach areas efficiently makes them an invaluable tool for maintaining structural integrity and safety in tall buildings.



Figure 1: UAV in operation for building inspection



1.2 Drone Scenarios for Inspection

The following scenarios outline critical performance benchmarks that directly support the safe and reliable execution of demanding building inspection tasks. Each highlights a specific challenge and its importance for the drone's operational integrity, alongside the practical contexts in which it's expected to occur.

1.2.1 Hovering from a Freehand Throw

This scenario demonstrates the UAV's ability to quickly establish its initial arbitrary attitude, position, and velocity from a non-standard launch, then rapidly damp oscillations and transition into stable hover. This fundamental capability shows the system's overall responsiveness and robustness. It represents the drone's capacity to quickly stabilize from highly unpredicted initial conditions or minor deployment anomalies, contributing to operational flexibility.

1.2.2 Hovering from a Free Fall

This scenario assesses the drone's ability to detect an uncontrolled descent—simulating loss of thrust and automatically initiate a recovery maneuver to arrest the fall and regain stable hover. Successful performance is essential for preventing catastrophic crashes and ensuring safety. This scenario could

occur due to unexpected system malfunctions such as motor/ESC failure or extreme environmental factors like sudden, severe downdrafts during inspection flights near tall buildings.

1.2.3 Hovering from an Upside-Down Orientation

This scenario rigorously tests the drone's attitude control authority and recovery dexterity. It requires the system to accurately identify an inverted state and execute a controlled maneuver to reorient itself to a stable, upright hovering position. This demonstrates the drone's resilience to unusual attitudes, enhancing mission continuity even after minor impacts or extreme flight conditions. An upside-down orientation might result from minor contact with complex architectural features or unforeseen obstacles during close-proximity maneuvers.

1.2.4 Maintaining Hover with Aggressive Inputs

This is a fundamental operational performance requirement for high-quality data acquisition during inspections. It evaluates the controller's ability to maintain precise hover despite significant external disturbances (e.g., strong wind gusts) or rapid, demanding pilot commands. Achieving this ensures captured imagery remains clear and accurate. This scenario is routinely encountered during building inspection operations where drones are exposed to turbulent airflow and unpredictable gusts.

1.2.5 Emergency Response within a Specific Timeframe

This represents the ultimate measure of the drone's safety and operational reliability in critical situations. It mandates that the drone can swiftly detect a severe hazard—such as an imminent collision or a critical system anomaly—and initiate a pre-programmed emergency response within a predefined, minimal time window. This capability is paramount for preventing accidents, protecting property, and ensuring compliance. This scenario covers any unforeseen critical event that demands immediate, decisive action, with the specified timeframe ensuring the drone can react before a dangerous situation escalates.

2 Literature Review

2.1 QuadrotorDrone components and system

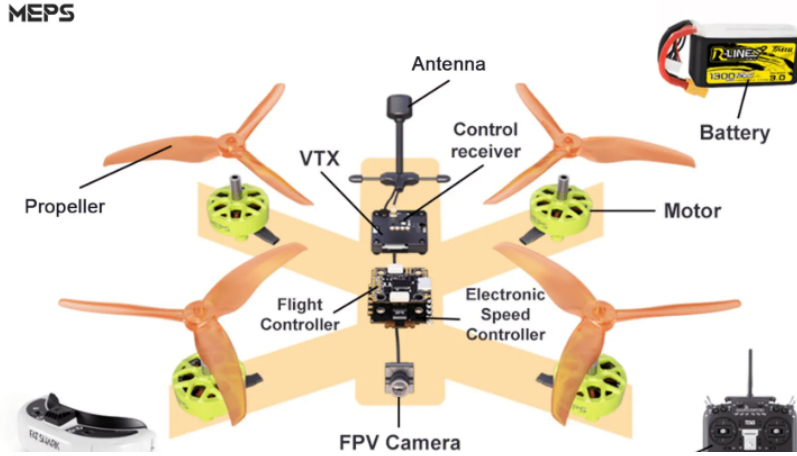


Figure 2: Labelled Quadrotor drone components

[2]

The quadrotor represents an integrated mechatronic system combining key subsystems: The plant (mechanical system) comprises four brushless motors and propellers that generate adjustable thrust vectors, along with the mechanical power system (MEPS) that ensures efficient energy transfer while minimizing vibrations. The control system centers on the flight control board executing PID algorithms, processing real-time data from inertial measurement units (IMUs) and barometric sensors (the sensing subsystem) to maintain stability against disturbances. The actuation system consists of electronic speed controllers (ESCs) that translate control signals into motor actions, while the power distribution network forms the energy subsystem. For human operation, the first-person-view (FPV) camera, video transmitter (VTX) and antenna create a human-machine interface subsystem providing low-latency visual feedback. This synergistic integration demonstrates core mechatronic principles - the precisely balanced interaction between the mechanical plant, electronic sensors, digital control algorithms, and power systems enables stable operation in dynamic environments. By replacing each component's function within the mechatronic framework, we achieve a reliable inspection platform that outperforms manual methods in safety and efficiency for high-rise structural assessments.

2.2 Quadrotor Model Assumptions

Wil Selby et al.[3] discuss common idealizing assumptions made to simplify quadrotor models, which are crucial for deriving manageable equations of motion. These assumptions typically include treating the quadrotor as a rigid body, implying its shape and mass distribution remain constant during flight. It's also often assumed to have a symmetrical mass distribution, simplifying calculations related to its moments of inertia.

2.3 Quadrotor System Modeling

Wil Selby's[3] quadrotor modeling approach applies nonlinear dynamics theory to develop a comprehensive mathematical model of drone motion. The work derives equations for 6-degree-of-freedom (6DOF) rigid body dynamics, incorporating thrust generation, torque effects, and environmental disturbances.

Key theoretical foundations include Newton-Euler mechanics for rotational dynamics and blade element theory for propeller aerodynamics. This modeling is particularly relevant for high-rise inspections as it enables precise simulation of wind disturbances and proximity effects - critical factors when operating near structures. The physics-based approach allows for control system development that maintains stability in turbulent urban environments. The model's fidelity supports development of robust control algorithms aligning with inspection drone requirements.

2.4 Design Objectives

The focus for this project is on designing a robust drone control system capable of performing critical high-rise inspection manoeuvres, including:

- Mid-air recovery from freehand throws, free falls, and inverted positions to enable rapid deployment and collision recovery.
- Aggressive disturbance rejection to maintain stable hover during wind gusts or operator over-corrections.
- Precision proximity flight for detailed facade, balcony, and emergency exit inspections.
- Obstacle resilience to safely navigate around building protrusions and structural elements.
- Obtain the nonlinear 6 DOF second order differential equations of a quadcopter (plant).
- Determine the behavior of the 12 states of the uncontrolled nonlinear plant with time to simple standard inputs (step, ramp, sinusoid, etc.).
- Linearize the plant equations about a single equilibrium hover position.
- Determine the behavior of the 12 states of the uncontrolled linear plant with time to standard inputs.
- Prove that a quadcopter is an underactuated plant that requires a controller to fly predictably.
- Use open-loop linear system tools to analytically study the stability of the system in detail.
- Use closed-loop linear system tools to analytically study the stability of the system in detail.
- Use time domain linear system tools to analytically study the stability of the system in detail.
- Use frequency domain linear system tools to analytically study the stability of the system in detail.
- Derive a scenario where both linear and nonlinear systems could be utilized.
- Use the scenario to derive realistic performance specifications.
- Design a PID controller using performance specifications.
- Design a controller analytically using Root Locus method.
- Test the controllers on both the controlled linear and nonlinear plant.
- Compare the results versus expectations using linear technique methods.
- Determine robustness of the linear controller in both linear and nonlinear regimes.
- Determine robustness of the linear controller under different initial conditions.

2.5 Problem Statement

The core challenge lies in developing control algorithms that can process real-time sensor data and execute rapid motor adjustments to maintain stability in these dynamic scenarios. This solution aims to bridge the gap between conventional drone capabilities and the demanding requirements of high-rise building inspections, providing a safer, more cost-effective alternative to manual methods while enabling more frequent and thorough structural assessments.

3 Performance Specifications

3.1 Time-domain Performance Specifications

The time domain specifications focus on how a system responds to an input over time. For linear systems, the principle of superposition allows for analysis of response to command inputs separately from the response to disturbances. When both occur simultaneously, the total system response is simply the sum of the individual responses. However, in nonlinear systems, this approach is not valid, as superposition does not apply. For the system, the performance is evaluated by simulating the response to a unit step input and considering the following characteristics.

- **Rise time (T_r)** is the time taken for the system's response to rise from 10% to 90% of its final value. This performance specification indicates how quickly the system responds to an input and it is usually required to be as small as possible.
- **Peak time (T_p)** is the time taken system's response to reach its first peak (maximum value). This performance specification helps assess the speed of system's response.
- **Maximum overshoot (M_p)** is the amount by which the response exceeds the final value. This specification indicates the system's tendency to exceed the desired value and too much overshoot can cause drone instability which is problem for inspection application.
- **Settling time (T_s)** is the time required for the system's response to remain within a certain percentage of its final value. This time is required to be small and the common values used are 2% and 5%. This specification measures the ability of the drone to stabilize quickly.
- **Steady-state error (E_{ss})** is the difference between the actual and the desired output. This specification measures the accuracy of the designed system.

The desired performance specifications in the time-domain are presented in Table 1 and were calculated using equations in the Appendix.

Table 1: Time-domain performance specifications

Specification	Value
Rise time (T_r)	2.5
Peak time (T_p)	3
Maximum overshoot (M_p)	7.5percent
Settling time (T_s)	7s
Steady-state error (E_{ss})	0

3.2 Frequency-domain Performance Specifications

Frequency domain performance specifications describe how a system responds to inputs at different frequencies. Unlike in time-domain where the system behaviour is examined over time, this domain is concerned with characteristics of system frequency response, which is important for analysing stability, robustness and performance of the system.

- **Amplitude ratio** is the ratio of the output amplitude to the input amplitude when an input is applied to the system. This ratio helps to evaluate how well the system filters signals.

- **Peak amplitude ratio** (M_p) is the maximum value of the amplitude ratio observed in the frequency response of the system. This value indicates the stability of the system and if it is too high it means excessive overshoot hence poor system's relative stability.
- **Resonant frequency** (ω_r) is the frequency at peak amplitude ratio. This specification is the speed of response criterion and high frequency response means fast speed of response.
- **Bandwidth** is the range of frequencies where the system amplitude ratio remains within acceptable level. A larger bandwidth indicates faster system's response and smaller bandwidth indicates slower system's response but more robust.

The desired performance specifications in the frequency-domain are presented in Table 2 and were calculated using equations in the Appendix.

Table 2: Quadrotor Model Specifications

Specification	Value
Amplitude ratio	0-1
Peak Amplitude ratio	1.1 - 1.5
Resonant Frequency	628.32rads/s
Bandwidth	125.66 - 628.32rads

4 Mathematical Model

4.1 Quadrotor Model Assumptions

The proposed system is a quadrotor UAV with a four-rotor, symmetrical frame designed for stable and responsive flight. Each rotor generates vertical thrust, and by adjusting individual motor speeds, the system achieves control over roll, pitch, yaw, and altitude. The frame is lightweight and rigid, supporting components such as motors, electronic speed controllers (ESCs), and Inertial Measurements Unit (IMU) sensors to provide real-time orientation of the drone. This section details the modelling of the system, providing a better understanding of how the system will operate and how it can be manipulated and controlled during destabilizing events.

4.1.1 Structural Assumptions

- **Rigid Body Dynamics:**

- The entire quadrotor (frame and propellers) is perfectly rigid with no deformation, flexing, or vibrations.
- The frame is perfectly symmetrical with uniform mass distribution.
- The center of mass coincides exactly with the geometric center of the frame, and payload movement is negligible.

- **Inertial Properties:**

- Products of inertia are zero: $I_{xy} = I_{xz} = I_{yz} = 0$.
- Moments of inertia about the x and y axes are equal: $I_{xx} = I_{yy}$.
- Propeller mass and inertia are negligible compared to the total drone mass.

4.1.2 Aerodynamic Assumptions

- **Propeller Dynamics:**

- All motor-propeller combinations are identical in performance.
- Thrust and drag torque are perfectly proportional to the square of the rotor's angular speed (ω^2), with no time delays or nonlinear effects.
- Thrust and drag coefficients are identical for all propellers.
- Gyroscopic effects from spinning propellers are negligible.

- **Environmental Simplifications:**

- Air resistance (drag), blade flapping, and ground effects are neglected in the basic model.

4.1.3 Control and Measurement Assumptions

- **Ideal Actuators and Sensors:**

- Electronic speed controllers (ESCs) respond instantaneously to control inputs without lag or saturation.
- The inertial measurement unit (IMU) provides noise-free, ideal readings of orientation and acceleration.

4.2 Mathematical Model

4.2.1 Reference Frames and Coordinate Transformations

The quadrotor's motion is described using two primary reference frames:

- **Inertial Frame (W)**: Earth-fixed frame with axes $\{X, Y, Z\}$ where $+Z$ points upward.
- **Body Frame (B)**: Attached to the quadrotor's center of mass with axes $\{x, y, z\}$ where $+z$ aligns with the thrust direction.

The orientation is defined using Euler angles (roll ϕ , pitch θ , yaw ψ) with Z-Y-X convention. The rotation matrix from body to inertial frame is:

$$\mathbf{R} = \mathbf{R}_z(\psi)\mathbf{R}_y(\theta)\mathbf{R}_x(\phi)$$

Assumptions:

- Rigid body with no structural deformation
- Symmetric mass distribution
- Center of mass coincides with geometric center

4.2.2 Forces and Moments Analysis

The system is subject to the following forces and moments:

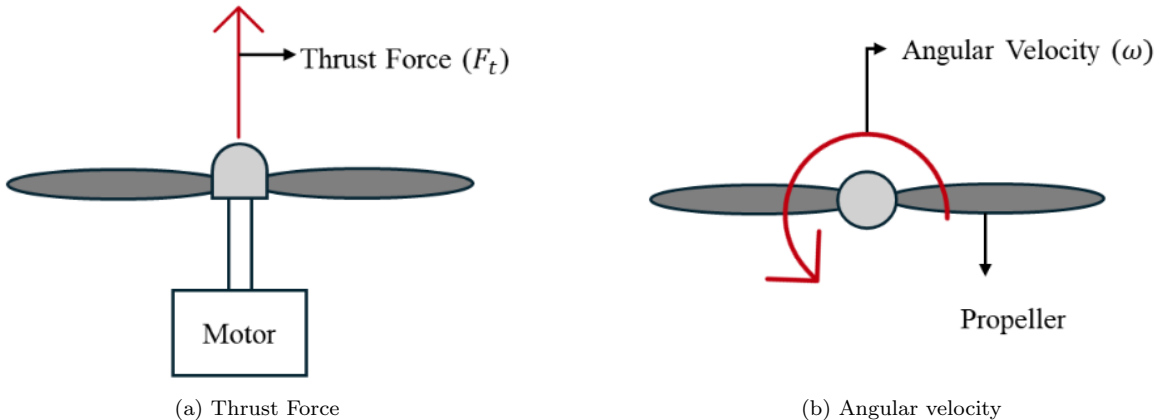


Figure 3: Insert Caption

- **Thrust** from each rotor:

$$F_i = k\omega_i^2 \quad (1)$$

where:

- F_i is the thrust force on the propeller (N)
- k is the thrust coefficient ($N \cdot s^2 / rad^2$)
- ω_i is the angular velocity of motor i (rad/s)

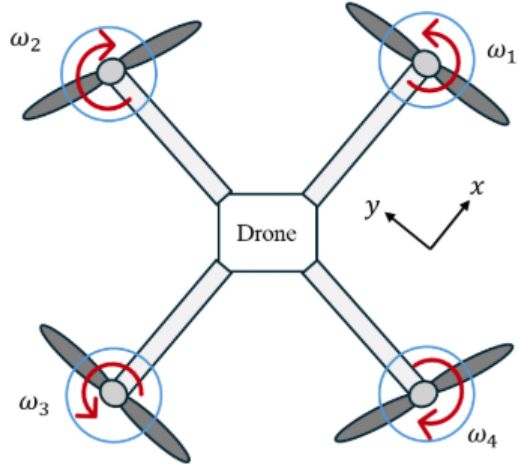


Figure 4: Drone Top view

The total thrust force generated by all motors:

$$F_T = \sum_{i=1}^4 k\omega_i^2 = k(\omega_1^2 + \omega_2^2 + \omega_3^2 + \omega_4^2) \quad (2)$$

- **Gravity:** $F_g = mg$ acting along $-Z$

- **Moments:**

- Roll moment (x -axis):

$$M_x = lk(\omega_2^2 - \omega_4^2) \quad (3)$$

- Pitch moment (y -axis):

$$M_y = lk(\omega_1^2 - \omega_3^2) \quad (4)$$

- Yaw moment (z -axis):

$$M_z = d(\omega_1^2 - \omega_2^2 + \omega_3^2 - \omega_4^2) \quad (5)$$

where l is the arm length and d is the drag coefficient.

4.3 Nonlinear Dynamics

4.3.1 Translational Dynamics

State variables: $x_1 = x$, $x_2 = \frac{dx}{dt}$, $x_3 = y$, $x_4 = \frac{dy}{dt}$, $x_5 = z$, $x_6 = \frac{dz}{dt}$

X-direction

$$\dot{x}_1 = x_2 \quad (6)$$

$$\dot{x}_2 = \frac{(\cos \theta \sin \phi \cos \psi + \sin \theta \sin \psi)U_1}{m} \quad (7)$$

Models the x-direction motion, with acceleration driven by thrust U_1 , orientation angles (θ, ϕ, ψ) , and mass m .

Y-direction

$$\dot{x}_3 = x_4 \quad (8)$$

$$\dot{x}_4 = \frac{(\cos \theta \sin \phi \sin \psi - \sin \theta \cos \psi)U_1}{m} \quad (9)$$

Describes the y-direction motion, similarly influenced by thrust and orientation.

Z-direction

$$\dot{x}_5 = x_6 \quad (10)$$

$$\dot{x}_6 = g + \frac{(\cos \theta \cos \phi)U_1}{m} \quad (11)$$

Represents the z-direction motion, including gravitational acceleration g and the vertical thrust component.

4.3.2 Rotational Dynamics

Roll State variables: $x_7 = \psi$, $x_8 = \frac{d\psi}{dt}$, $x_9 = \theta$, $x_{10} = \frac{d\theta}{dt}$, $x_{11} = \phi$, $x_{12} = \frac{d\phi}{dt}$

$$\dot{x}_7 = x_8 \quad (12)$$

$$\dot{x}_8 = \frac{(I_{yy} - I_{zz})\dot{\theta}\dot{\phi} - J_r\dot{\theta}\Omega + U_2}{I_{xx}} \quad (13)$$

Yaw dynamics, with angular acceleration influenced by moments of inertia, gyroscopic effects ($J_r\Omega$), and control input U_2 .

Pitch

$$\dot{x}_9 = x_{10} \quad (14)$$

$$\dot{x}_{10} = \frac{(I_{zz} - I_{xx})\dot{\psi}\dot{\phi} + U_3}{I_{yy}} \quad (15)$$

Pitch dynamics, driven by inertial differences and control input U_3 .

Yaw

$$\dot{x}_{11} = x_{12} \quad (16)$$

$$\dot{x}_{12} = \frac{(I_{xx} - I_{yy})\dot{\psi}\dot{\theta} - J_r\dot{\psi}\Omega + U_4}{I_{zz}} \quad (17)$$

Roll dynamics, with similar inertial and gyroscopic terms, and control input U_4 .

4.3.3 Control Inputs

$$U_1 = k(\omega_1^2 + \omega_2^2 + \omega_3^2 + \omega_4^2) \quad (18)$$

$$U_2 = lk(-\omega_1^2 + \omega_2^2 - \omega_3^2 + \omega_4^2) \quad (19)$$

$$U_3 = lk(-\omega_1^2 - \omega_2^2 + \omega_3^2 + \omega_4^2) \quad (20)$$

$$U_4 = d(-\omega_1^2 + \omega_2^2 - \omega_3^2 + \omega_4^2) \quad (21)$$

Where m is the mass of the quadcopter, g is the gravitational acceleration, I_{xx} is the moment of inertia

about x-axis, I_{yy} is the moment of inertia about y-axis, I_{zz} is the moment of inertia about z-axis, k is the thrust factor, d is the drag factor, l is the length of the rotor arm, JTP is the rotor moment of inertia, and ω are the rotor speeds. This mathematical model establishes the basis for the control design and optimization discussed in the subsequent sections.

4.4 Linear Model

4.4.1 Translational Dynamics

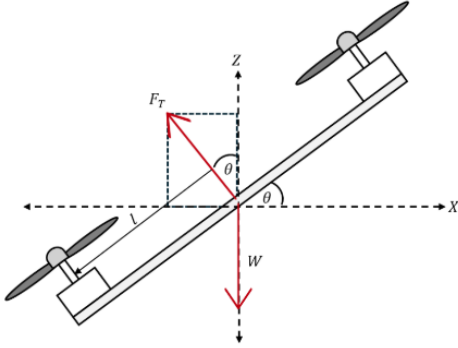


Figure 5: Quadrotor axis and parameters

X-direction Variables: $\dot{x}_1, \dot{x}_2, x_2, \theta, \phi, U_1$

Equilibrium point: $x_{20} = 0; \dot{x}_{10} = 0; \dot{x}_{20} = 0; \theta_0 = 0; \phi_0 = 0; \psi_0 = 0; U_{10} = mg$

$$f_1 = \dot{x}_1 - x_2 = 0 \quad (22)$$

$$f_{10} = \dot{x}_{10} - x_{20} = 0 \quad (23)$$

$$\left. \frac{df_1}{dx_1} \right|_e \Delta x_1 = \Delta \dot{x}_1; \left. \frac{df_1}{dx_2} \right|_e \Delta x_2 = -\Delta x_2; \left. \frac{df_1}{d\dot{x}_2} \right|_e \Delta \dot{x}_2 = 0; \quad (24)$$

$$\left. \frac{df_1}{dU_1} \right|_e \Delta U_1 = 0; \left. \frac{df_1}{d\theta} \right|_e \Delta \theta = 0; \left. \frac{df_1}{d\phi} \right|_e \Delta \phi = 0; \left. \frac{df_1}{d\psi} \right|_e \Delta \psi = 0 \quad (25)$$

$$\Delta x_1 = \Delta x_2 \quad (26)$$

$$f_2 = \dot{x}_2 - (\cos \theta \sin \phi \cos \psi + \sin \theta \sin \psi) \frac{U_1}{m} = 0 \quad (27)$$

$$f_{20} = \dot{x}_{20} - (\cos \theta_0 \sin \phi_0 \cos \psi_0 + \sin \theta_0 \sin \psi_0) \frac{U_{10}}{m} = 0 \quad (28)$$

$$\left. \frac{df_2}{dx_1} \right|_e \Delta x_1 = 0; \left. \frac{df_2}{dx_2} \right|_e \Delta x_2 = 0; \left. \frac{df_2}{d\dot{x}_2} \right|_e \Delta \dot{x}_2 = \Delta \dot{x}_2; \left. \frac{df_2}{dU_1} \right|_e \Delta U_1 = 0; \quad (29)$$

$$\left. \frac{df_2}{d\theta} \right|_e \Delta \theta = -\frac{U_{10}}{m} \sin \phi_0 \Delta \theta; \left. \frac{df_2}{d\phi} \right|_e \Delta \phi = -\frac{U_{10}}{m} \cos \phi_0 \Delta \phi; \left. \frac{df_2}{d\psi} \right|_e \Delta \psi = 0 \quad (30)$$

$$\Delta \dot{x}_2 = g \sin \phi_0 \Delta \theta + g \cos \phi_0 \Delta \phi \quad (31)$$

Y-direction Variables: $\dot{x}_3, \dot{x}_4, x_4, \theta, \phi, U_1$

Equilibrium point: $x_{40} = 0; x_{30} = 0; \dot{x}_{40} = 0; \theta_0 = 0; \phi_0 = 0; \psi_0 = 0; U_{10} = mg$

$$f_3 = \dot{x}_3 - x_4 = 0 \quad (32)$$

$$f_{30} = \dot{x}_{30} - x_{40} = 0 \quad (33)$$

$$\frac{df_3}{dx_3} \Big|_e \Delta x_3 = \Delta \dot{x}_3; \frac{df_3}{dx_4} \Big|_e \Delta x_4 = -\Delta x_4; \frac{df_3}{d\dot{x}_4} \Big|_e \Delta \dot{x}_4 = 0; \quad (34)$$

$$\frac{df_3}{dU_1} \Big|_e \Delta U_1 = 0; \frac{df_3}{d\emptyset} \Big|_e \Delta \emptyset = 0; \frac{df_3}{d\theta} \Big|_e \Delta \theta = 0; \frac{df_3}{d\phi} \Big|_e \Delta \phi = 0 \quad (35)$$

$$\Delta \dot{x}_3 = \Delta x_4 \quad (36)$$

$$f_4 = \dot{x}_4 - (\cos \emptyset \sin \theta \sin \phi + \sin \emptyset \sin \phi) \frac{U_1}{m} = 0 \quad (37)$$

$$f_{40} = \dot{x}_{40} - (\cos \emptyset_0 \sin \theta_0 \sin \phi_0 + \sin \emptyset_0 \sin \phi_0) \frac{U_{10}}{m} = 0 \quad (38)$$

$$\frac{df_4}{dx_3} \Big|_e \Delta x_3 = 0; \frac{df_4}{dx_4} \Big|_e \Delta x_4 = 0; \frac{df_4}{d\dot{x}_4} \Big|_e \Delta \dot{x}_4 = \Delta \dot{x}_4; \frac{df_4}{dU_1} \Big|_e \Delta U_1 = 0; \quad (39)$$

$$\frac{df_4}{d\emptyset} \Big|_e \Delta \emptyset = -\frac{U_{10}}{m} \sin \theta_0 \Delta \emptyset; \frac{df_4}{d\theta} \Big|_e \Delta \theta = -\frac{U_{10}}{m} \sin \theta_0 \Delta \theta; \frac{df_4}{d\phi} \Big|_e \Delta \phi = 0 \quad (40)$$

$$\Delta \dot{x}_4 = g \sin \theta_0 \Delta \emptyset + g \sin \theta_0 \Delta \theta \quad (41)$$

Z-direction

Variables: $\dot{x}_5, \dot{x}_6, x_6, \emptyset, \theta, U_1$

Equilibrium point: $x_{60} = 0; \dot{x}_{50} = 0; \dot{x}_{60} = 0; \emptyset_0 = 0; \theta_0 = 0; U_{10} = mg$

$$f_5 = \dot{x}_5 - x_6 = 0 \quad (42)$$

$$f_{50} = \dot{x}_{50} - x_{60} = 0 \quad (43)$$

$$\frac{df_5}{dx_5} \Big|_e \Delta x_5 = \Delta \dot{x}_5; \frac{df_5}{dx_6} \Big|_e \Delta x_6 = -\Delta x_6; \frac{df_5}{d\dot{x}_6} \Big|_e \Delta \dot{x}_6 = 0; \quad (44)$$

$$\frac{df_5}{dU_1} \Big|_e \Delta U_1 = 0; \frac{df_5}{d\emptyset} \Big|_e \Delta \emptyset = 0; \frac{df_5}{d\theta} \Big|_e \Delta \theta = 0 \quad (45)$$

$$\Delta \dot{x}_5 = \Delta x_6 \quad (46)$$

$$f_6 = \dot{x}_6 + g - \cos \emptyset \cos \theta \frac{U_1}{m} = 0 \quad (47)$$

$$f_{60} = \dot{x}_{60} + g - \cos \emptyset_0 \cos \theta_0 \frac{U_{10}}{m} = 0 \quad (48)$$

$$\frac{df_6}{dx_5} \Big|_e \Delta x_5 = 0; \frac{df_6}{dx_6} \Big|_e \Delta x_6 = 0; \frac{df_6}{d\dot{x}_6} \Big|_e \Delta \dot{x}_6 = \Delta \dot{x}_6; \quad (49)$$

$$\frac{df_6}{dU_1} \Big|_e \Delta U_1 = -\frac{1}{m} U_1; \frac{df_6}{d\emptyset} \Big|_e \Delta \emptyset = 0; \frac{df_6}{d\theta} \Big|_e \Delta \theta = 0 \quad (50)$$

$$\Delta \dot{x}_6 = \frac{1}{m} U_1 \quad (51)$$

4.4.2 Roll

Variables: $\dot{x}_7, \dot{x}_8, x_8, U_2$

Equilibrium point: $\dot{x}_{80} = 0; \dot{x}_{70} = 0; \dot{x}_{80} = 0; \theta_0 = 0; \phi_0 = 0; U_{20} = 0; \omega_0 \neq 0$

$$f_7 = \dot{x}_7 - x_8 = 0 \quad (52)$$

$$f_{70} = \dot{x}_{70} - \dot{x}_{80} = 0 \quad (53)$$

$$\frac{df_7}{dx_7} \Big|_e \Delta x_7 = \Delta \dot{x}_7; \frac{df_7}{dx_8} \Big|_e \Delta x_8 = -\Delta x_8; \frac{df_7}{d\dot{x}_8} \Big|_e \Delta \dot{x}_8 = 0; \quad (54)$$

$$\frac{df_7}{dU_2} \Big|_e \Delta U_2 = 0; \frac{df_7}{d\theta} \Big|_e \Delta \theta = 0; \frac{df_7}{d\phi} \Big|_e \Delta \phi = 0; \frac{df_7}{d\psi} \Big|_e \Delta \psi = 0 \quad (55)$$

$$\Delta \dot{x}_7 = \Delta x_8 \quad (56)$$

$$f_8 = \dot{x}_8 - (I_{YY} - I_{ZZ}) - J_{TP}\omega + \frac{U_2}{I_{XX}} = 0 \quad (57)$$

$$f_{80} = \dot{x}_{80} - (I_{YY} - I_{ZZ})00 - J_{TP}0\omega_0 + \frac{U_{20}}{I_{XX}} = 0 \quad (58)$$

$$\frac{df_8}{dx_7} \Big|_e \Delta x_7 = 0; \frac{df_8}{dx_8} \Big|_e \Delta x_8 = 0; \frac{df_8}{d\dot{x}_8} \Big|_e \Delta \dot{x}_8 = \Delta \dot{x}_8; \quad (59)$$

$$\frac{df_8}{dU_2} \Big|_e \Delta U_2 = -\frac{1}{I_{XX}} \Delta U_2; \frac{df_8}{d\theta} \Big|_e \Delta \theta = \frac{J_{TP}\omega_0}{I_{XX}} \Delta \theta; \frac{df_8}{d\phi} \Big|_e \Delta \phi = 0; \frac{df_8}{d\psi} \Big|_e \Delta \psi = 0 \quad (60)$$

$$\Delta \dot{x}_8 = \frac{1}{I_{XX}} \Delta U_2 - \frac{J_{TP}\omega_0}{I_{XX}} \Delta \theta \quad (61)$$

4.4.3 Pitch

Variables: $\dot{x}_9, \dot{x}_{10}, x_{10}, \emptyset, U_3$

Equilibrium point: $\dot{x}_{100} = 0; \dot{x}_{90} = 0; \dot{x}_{100} = 0; \emptyset_0 = 0; \theta_0 = 0; U_{30} = 0; \omega_0 \neq 0$

$$f_9 = \dot{x}_9 - x_{10} = 0 \quad (62)$$

$$f_{90} = \dot{x}_{90} - \dot{x}_{100} = 0 \quad (63)$$

$$\frac{df_9}{dx_9} \Big|_e \Delta x_9 = \Delta \dot{x}_9; \frac{df_9}{dx_{10}} \Big|_e \Delta x_{10} = -\Delta x_{10}; \frac{df_9}{d\dot{x}_{10}} \Big|_e \Delta \dot{x}_{10} = 0; \quad (64)$$

$$\frac{df_9}{dU_3} \Big|_e \Delta U_3 = 0; \frac{df_9}{d\emptyset} \Big|_e \Delta \emptyset = 0; \frac{df_9}{d\theta} \Big|_e \Delta \theta = 0; \frac{df_9}{d\phi} \Big|_e \Delta \phi = 0 \quad (65)$$

$$\Delta \dot{x}_9 = \Delta x_{10} \quad (66)$$

$$f_{10} = \dot{x}_{10} - (I_{ZZ} - I_{XX})\emptyset - J_{TP}\emptyset\omega + \frac{U_3}{I_{YY}} = 0 \quad (67)$$

$$f_{100} = \dot{x}_{100} - (I_{ZZ} - I_{XX})\emptyset_00 - J_{TP}\emptyset_0\omega_0 + \frac{U_{30}}{I_{YY}} = 0 \quad (68)$$

$$\frac{df_{10}}{dx_9} \Big|_e \Delta x_9 = 0; \frac{df_{10}}{dx_{10}} \Big|_e \Delta x_{10} = 0; \frac{df_{10}}{d\dot{x}_{10}} \Big|_e \Delta \dot{x}_{10} = \Delta \dot{x}_{10}; \quad (69)$$

$$\frac{df_{10}}{dU_3} \Big|_e \Delta U_3 = -\frac{1}{I_{YY}} \Delta U_3; \frac{df_{10}}{d\emptyset} \Big|_e \Delta \emptyset = \frac{J_{TP}\omega_0}{I_{YY}} \Delta \emptyset; \frac{df_{10}}{d\theta} \Big|_e \Delta \theta = 0; \frac{df_{10}}{d\phi} \Big|_e \Delta \phi = 0 \quad (70)$$

$$\Delta \dot{x}_{10} = \frac{1}{I_{YY}} \Delta U_3 - \frac{J_{TP}\omega_0}{I_{YY}} \Delta \emptyset \quad (71)$$

4.4.4 Yaw

Variables: $\dot{x}_{11}, \dot{x}_{12}, x_{12}, \emptyset, U_4$

Equilibrium point: $\dot{x}_{120} = 0; \dot{x}_{110} = 0; \dot{x}_{120} = 0; \theta_0 = 0; \emptyset_0 = 0; U_{40} = 0$

$$f_{11} = \dot{x}_{11} - x_{12} = 0 \quad (72)$$

$$f_{110} = \dot{x}_{110} - \dot{x}_{120} = 0 \quad (73)$$

$$\frac{df_{11}}{dx_{11}} \Big|_e \Delta x_{11} = \Delta \dot{x}_{11}; \frac{df_{11}}{dx_{12}} \Big|_e \Delta x_{12} = -\Delta x_{12}; \frac{df_{11}}{d\dot{x}_{12}} \Big|_e \Delta \dot{x}_{12} = 0; \quad (74)$$

$$\frac{df_{11}}{dU_4} \Big|_e \Delta U_4 = 0; \frac{df_{11}}{d\emptyset} \Big|_e \Delta \emptyset = 0; \frac{df_{11}}{d\theta} \Big|_e \Delta \theta = 0 \quad (75)$$

$$\Delta \dot{x}_{11} = \Delta x_{12} \quad (76)$$

$$f_{12} = \dot{x}_{12} - (I_{XX} - I_{YY})\emptyset + \frac{U_4}{I_{ZZ}} = 0 \quad (77)$$

$$f_{120} = \dot{x}_{120} - (I_{XX} - I_{YY})\emptyset_0 0 + \frac{U_{40}}{I_{ZZ}} = 0 \quad (78)$$

$$\frac{df_{12}}{dx_{11}} \Big|_e \Delta x_{11} = 0; \frac{df_{12}}{dx_{12}} \Big|_e \Delta x_{12} = 0; \frac{df_{12}}{d\dot{x}_{12}} \Big|_e \Delta \dot{x}_{12} = \Delta \dot{x}_{12}; \quad (79)$$

$$\frac{df_{12}}{dU_4} \Big|_e \Delta U_4 = \frac{1}{I_{ZZ}} \Delta U_4; \frac{df_{12}}{d\emptyset} \Big|_e \Delta \emptyset = 0; \frac{df_{12}}{d\theta} \Big|_e \Delta \theta = 0 \quad (80)$$

$$\Delta \dot{x}_{12} = \frac{1}{I_{ZZ}} \Delta U_4 \quad (81)$$

4.5 Equations of Motions for the System in Time-Domain and Frequency Domain

Table 3: Equations of Motions for the System in Time-Domain and Frequency Domain

Time-domain	Frequency-domain
$\Delta\dot{x}_1 = \Delta x_2$	$sX_1(s) = X_2(s)$
$\Delta\dot{x}_2 = g \sin \theta_0 \Delta\theta + g \cos \theta_0 \Delta\theta$	0
$\Delta\dot{x}_3 = \Delta x_4$	$sX_3(s) = X_4(s)$
$\Delta\dot{x}_4 = g \sin \theta_0 \Delta\theta + g \sin \theta_0 \Delta\theta$	0
$\Delta\dot{x}_5 = \Delta x_6$	$sX_5(s) = X_6(s)$
$\Delta\dot{x}_6 = \frac{1}{m}U_1$	$sX_6(s) = \frac{1}{m}U_1(s)$
$\Delta\dot{x}_7 = \Delta x_8$	$sX_7(s) = X_8(s)$
$\Delta\dot{x}_8 = \frac{1}{I_{XX}}\Delta U_2 - \frac{JTP\omega_0}{I_{XX}}\Delta\theta$	$sX_8(s) = \frac{1}{I_{XX}}U_2(s)$
$\Delta\dot{x}_9 = \Delta x_{10}$	$sX_9(s) = X_{10}(s)$
$\Delta\dot{x}_{10} = \frac{1}{I_{YY}}\Delta U_3 - \frac{JTP\omega_0}{I_{YY}}\Delta\theta$	$sX_{10}(s) = \frac{1}{I_{YY}}U_3(s)$
$\Delta\dot{x}_{11} = \Delta x_{12}$	$sX_{11}(s) = X_{12}(s)$
$\Delta\dot{x}_{12} = \frac{1}{I_{ZZ}}\Delta U_4$	$sX_{12}(s) = \frac{1}{I_{ZZ}}U_4(s)$

4.5.1 Transfer Functions of the System

$$T_s = \frac{\text{Output}}{\text{Input}}$$

4.5.2 Elevation

$$T_s = \frac{X_5(s)}{U_1(s)}$$

$$sX_5(s) = X_6 \quad (A) \quad sX_6(s) = \frac{1}{m}U_1(s) \quad (B) \quad (82)$$

Substituting the equations and rearranging to the transfer function format we get:

$$\frac{X_5(s)}{U_1(s)} = \frac{1}{ms^2} \quad (83)$$

In this transfer function the input is thrust control and the output is elevation.

4.5.3 Roll

$$T_s = \frac{X_7(s)}{U_2(s)}$$

$$sX_7(s) = X_8(s) \quad sX_8(s) = \frac{1}{I_{XX}}U_2(s) \quad (84)$$

Substituting equations above and rearranging to the transfer function format we get:

$$\frac{X_7(s)}{U_2(s)} = \frac{1}{I_{XX}s^2} \quad (85)$$

In this transfer function the input is roll and the output is roll.

4.5.4 Pitch

$$T_s = \frac{X_9(s)}{U_3(s)}$$

$$sX_9(s) = X_{10}(s) \quad sX_{10}(s) = \frac{1}{I_{YY}}U_3(s) \quad (86)$$

Substituting the equations above and rearranging to the transfer function format we get:

$$\frac{X_9(s)}{U_3(s)} = \frac{1}{I_{YY}s^2} \quad (87)$$

In this transfer function the input is pitch control and the output is pitch.

4.5.5 Yaw

$$T_s = \frac{X_{11}(s)}{U_4(s)}$$

$$sX_{11}(s) = X_{12}(s) \quad sX_{12}(s) = \frac{1}{I_{ZZ}}U_4(s) \quad (88)$$

Substituting the equations above and rearranging to the transfer function format we get:

$$\frac{X_{11}(s)}{U_4(s)} = \frac{1}{I_{ZZ}s^2} \quad (89)$$

In this transfer function the input is yaw control and the output is yaw.

Table 4: System Parameters

Parameter	Description	Value
m	Mass	0.506 kg
g	Gravitational acceleration	9.81 m/s ²
I_{XX}	Moment of inertia about the x-axis	8.12e-5 kgm ²
I_{YY}	Moment of inertia about the y-axis	8.12e-5 kgm ²
I_{ZZ}	Moment of inertia about the z-axis	6.12e-5 kgm ²
k	Thrust factor	3.13e-5
d	Drag factor	75e-7
J_{TP}	Rotor Moment of Inertia	6e-5 kgm ²
l	Length of the Rotor arm	0.235 m

4.6 State-Space Representation of Quadrotor Dynamics

State Vector

$$\mathbf{x} = \begin{bmatrix} x_1 \\ x_2 \\ x_3 \\ x_4 \\ x_5 \\ x_6 \\ x_7 \\ x_8 \\ x_9 \\ x_{10} \\ x_{11} \\ x_{12} \end{bmatrix} = \begin{bmatrix} x \\ \dot{x} \\ y \\ \dot{y} \\ z \\ \dot{z} \\ \psi \\ \dot{\psi} \\ \theta \\ \dot{\theta} \\ \phi \\ \dot{\phi} \end{bmatrix}$$

State-Space Equations

$$\dot{\mathbf{x}} = A\mathbf{x} + B\mathbf{u}$$

$$\mathbf{y} = C\mathbf{x} + D\mathbf{u}$$

4.6.1 System Matrix (A)

$$A = \left[\begin{array}{cccccccccc} 0 & 1 & 0 & 0 & 0 & 0 & 0 & 0 & 0 & 0 \\ 0 & 0 & & & & & & & & \\ 0 & 0 & 0 & 0 & 0 & 0 & 0 & 0 & g \cos \theta_0 & 0 \\ g \sin \theta_0 & 0 & & & & & & & & \\ 0 & 0 & 0 & 1 & 0 & 0 & 0 & 0 & 0 & 0 \\ 0 & 0 & & & & & & & & \\ 0 & 0 & 0 & 0 & 0 & 0 & 0 & 0 & g \sin \theta_0 & 0 \\ g \sin \theta_0 & 0 & & & & & & & & \\ 0 & 0 & 0 & 0 & 0 & 1 & 0 & 0 & 0 & 0 \\ 0 & 0 & & & & & & & & \\ 0 & 0 & 0 & 0 & 0 & 0 & 0 & 0 & 0 & 0 \\ 0 & 0 & & & & & & & & \\ 0 & 0 & 0 & 0 & 0 & 0 & 0 & 1 & 0 & 0 \\ 0 & 0 & & & & & & & & \\ 0 & 0 & 0 & 0 & 0 & 0 & 0 & 0 & -\frac{J_{TP}\omega_0}{I_{XX}} & \\ 0 & 0 & & & & & & & & \\ 0 & 0 & 0 & 0 & 0 & 0 & 0 & 0 & 1 & \\ 0 & 0 & & & & & & & & \\ 0 & 0 & 0 & 0 & 0 & 0 & 0 & 0 & 0 & 0 \\ 0 & -\frac{J_{TP}\omega_0}{I_{YY}} & & & & & & & & \\ 0 & 0 & 0 & 0 & 0 & 0 & 0 & 0 & 0 & 0 \\ 0 & 1 & & & & & & & & \\ 0 & 0 & 0 & 0 & 0 & 0 & 0 & 0 & 0 & 0 \\ 0 & 0 & & & & & & & & \end{array} \right]$$

Input Matrix (B)

$$B = \begin{bmatrix} 0 & 0 & 0 & 0 \\ 0 & 0 & 0 & 0 \\ 0 & 0 & 0 & 0 \\ 0 & 0 & 0 & 0 \\ 0 & 0 & 0 & 0 \\ \frac{1}{m} & 0 & 0 & 0 \\ 0 & 0 & 0 & 0 \\ 0 & \frac{1}{I_{XX}} & 0 & 0 \\ 0 & 0 & 0 & 0 \\ 0 & 0 & \frac{1}{I_{YY}} & 0 \\ 0 & 0 & 0 & 0 \\ 0 & 0 & 0 & \frac{1}{I_{ZZ}} \end{bmatrix}$$

Input Vector

$$\mathbf{u} = \begin{bmatrix} U_1 \\ U_2 \\ U_3 \\ U_4 \end{bmatrix}$$

Output Matrices

$$C = I_{12 \times 12}, \quad D = 0_{12 \times 4}$$

Uncontrolled Model Block Diagram

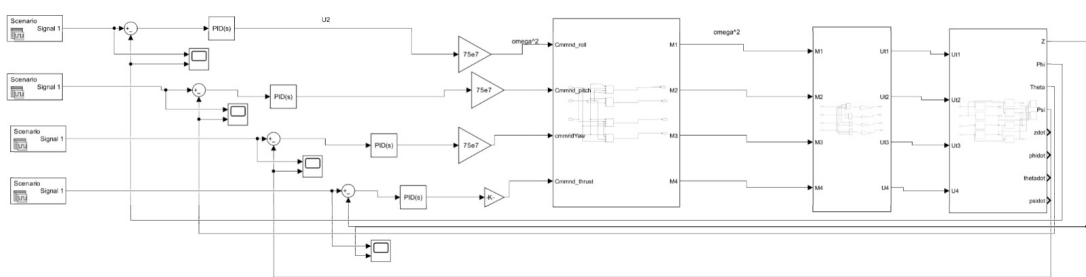


Figure 6: Overall Plant Block Diagram

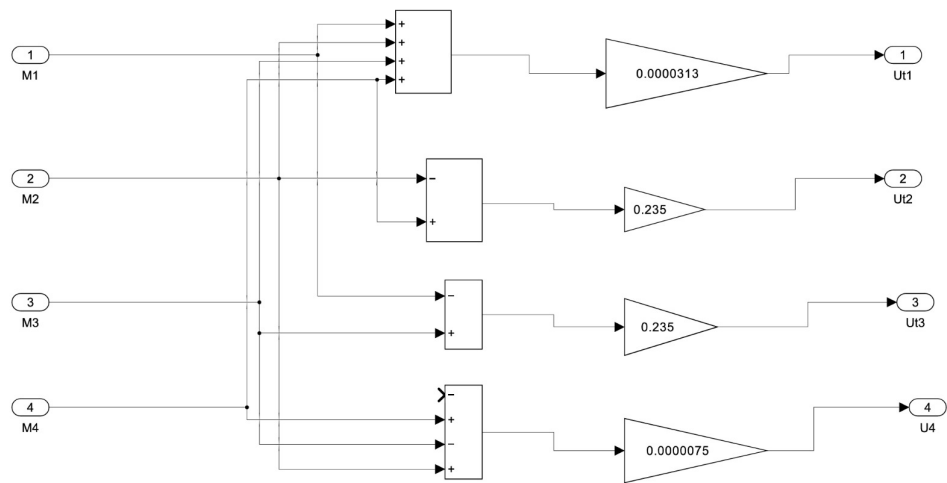


Figure 7: Linear Model Block Diagram

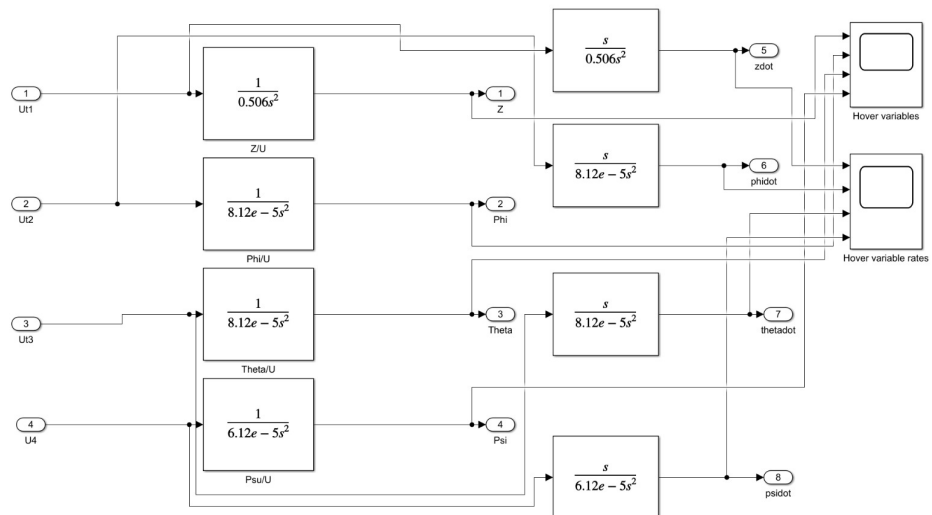


Figure 8: Linear Block diagram s-domain

5 System Response Analysis

To analyse the response of the system, the analytical equations that were derived in the previous section are used. The analysis is done for both non-linear uncontrolled plant and linearized version. The system is analysed using Matlab code and the responses are presented in this section.

5.1 Non-linear Plant

A non-linear plant refers to the system whose behaviour does not follow the principle of superposition meaning that its outputs do not vary linearly with respect to its inputs [5]. Since the system is non-linear in nature, for analysis it requires non-linear models. The non-linear analysis was done using the Matlab code and the mathematical models generated in time-domain were used for analysis. For the analysis the outputs are flight dynamics which are elevation, roll, pitch and yaw and the inputs are different control inputs where U_1 is the vertical control without any rotational control, U_2 is the roll control, U_3 is the pitch control and U_4 is the yaw control.

5.1.1 Non-linear Time-response of the System

Figure 9 presents the response of the non-linear plant when it is disturbed with the step input. The step input means to suddenly change the input from one value to another at a specified time and then stays at that value indefinitely. This input represents a sudden change in input commands, such as a change in desired elevation, roll, pitch, or yaw, and allows for the analysis of how the system responds to these disturbances. In the Figure, the first row shows the system's response in elevation, roll, pitch, and yaw when the step input for elevation which is U_1 is added to the system, the second row shows the system's response for the step input of roll, U_2 , third row shows the system's response for the step input of pitch, U_3 , and the last row shows the response when the yaw input, U_4 , is added to the system.

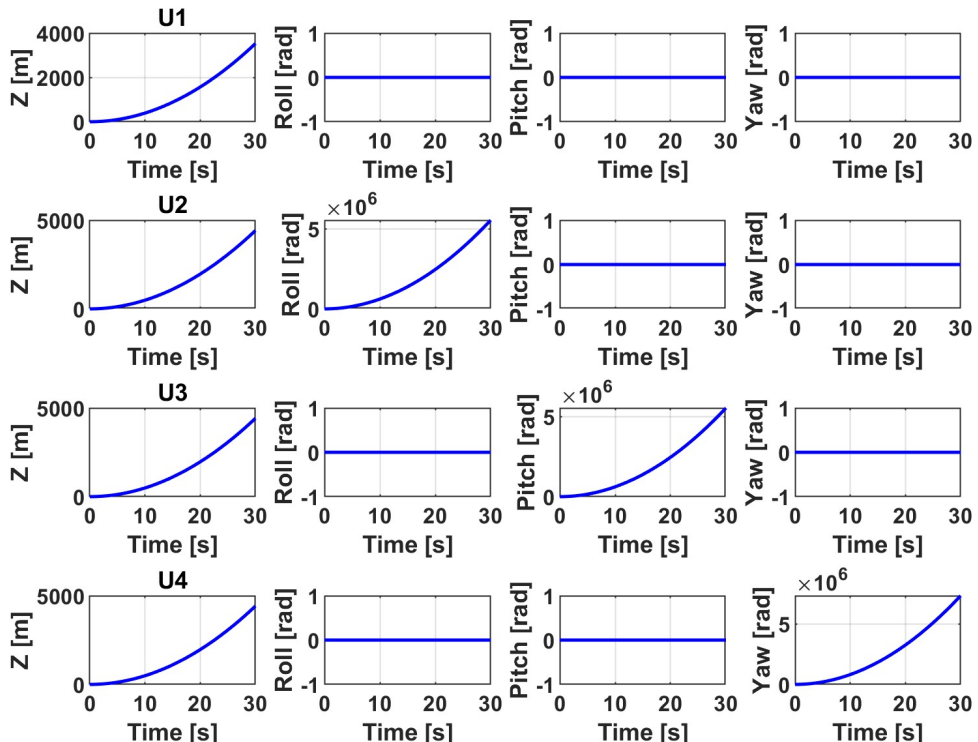


Figure 9: System non-linear response

In the Figure, all the graphs show the same exponential shape, indicating that when a step input is applied to the system, the response continues to grow without bound over time instead of settling to a steady-state value. This exponential growth is a clear sign of instability. Rather than returning to a new equilibrium, the system response keeps increasing, meaning it cannot effectively stabilize after disturbance. This behaviour suggests that the system is unable to maintain stable equilibrium after the step input.

5.2 System Response Analysis

5.2.1 Linear Plant

The non-linear plant was linearized using an analytical method to obtain the time-domain responses of the system's dynamics. This linearization simplifies the system by approximating the nonlinear equations with linear ones, allowing for easier analysis and prediction of the system's behaviour under various conditions [7]. By linearizing the system, the stability and time response can be analysed more effectively, providing better understanding into how the system behaves in response to inputs. The impulse and step inputs were used to evaluate the response of the system.

5.2.2 Linear Time Response of the System to the Impulse Input

The time response of the linearized system was evaluated using an impulse input, which is used to represent an instantaneous disturbance, and it helps to test the system's absolute stability; for instance, when it is momentarily disturbed, whether it will return to equilibrium or not. The results for this analysis are presented in Figure 10.

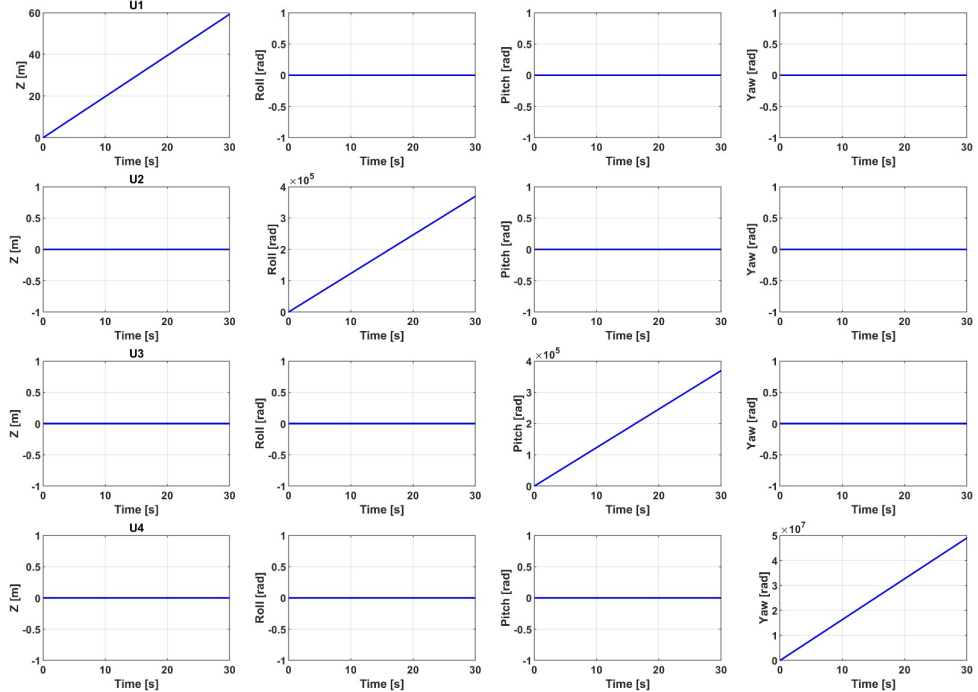


Figure 10: Impulse Input linear response

When the impulse input is applied to the system, the system is expected to experience a sudden change corresponding to the magnitude of the impulse, followed by a return to equilibrium. However, the figures show diverging responses, with the graphs increasing linearly without bound. When U_1 is applied, the system responds with a gradual increase in elevation while roll, pitch and yaw remain at zero meaning

that this input only affects vertical movement. U2 causes a rapid diverging response in roll angle while U3 and U4 cause rapid diverging response in pitch and yaw while other dynamics remains unaffected. This diverging response indicates that the system cannot maintain stability in all flight dynamics.

5.2.3 Linear time response of the system to the step input

The time response of the linearized system was also evaluated using a step input, which is used to represent a sustained change in input, and it helps to assess the system's ability to reach a new steady state after a disturbance, allowing for evaluation of the system's performance. The results for this analysis are presented in Figure 11.

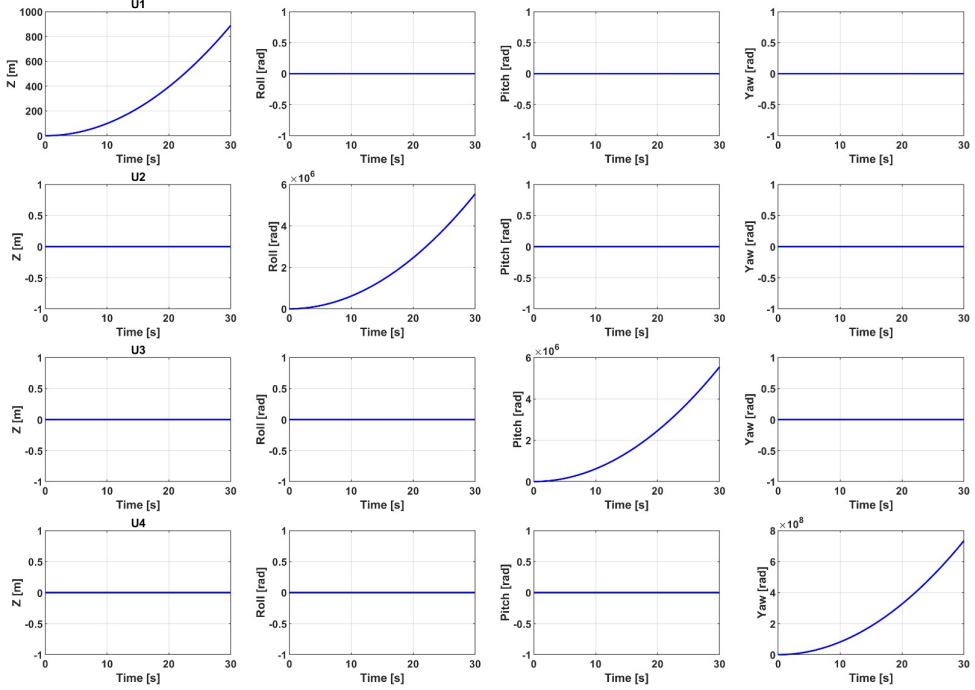


Figure 11: Step response of the linear system

When a step input is applied to the system, the system is expected to cause a sudden change corresponding to the magnitude of the step input, followed by a gradual stabilization at a new equilibrium. However, the figures also show diverging responses as of impulse input, with the graphs increasing exponential without bound, indicating instability in all flight dynamics.

5.2.4 Comparison of non-linear and linear uncontrolled models

For the linear uncontrolled model, the response of the system was analysed using two inputs: impulse and step input. These inputs were used to evaluate system response in the time-domain and stability. The impulse input provided better understanding into how the system reacts to a sudden, short-duration disturbance, while the step input revealed the system's response to a sustained change, showing its ability to reach a new steady-state. The results indicate instability, with the system's responses diverging without bound. Specifically, the impulse response shows a linear, unbounded increase for all flight dynamics, while the step response shows exponential, unbounded increase which is clear sign of unstable system. These findings highlight the lack of ability to maintain stability by the linear model.

The linear plant model is developed to replace the original non-linear plant model for improved simplicity in analysis. For the time responses of the flight dynamics, both linear and non-linear models follow the

same trend, indicating that the linear approximation closely matches the non-linear response. This correlation confirms the validity of the linear model within the considered operating conditions, implying that it can reliably replace the non-linear model for further analysis. When looking closely to both plant responses, when U2, U3, and U4 is applied to the system, for non-linear plant the elevation also responds, while for linear model it does not respond. This apparent difference is due to the presence of coupling in the non-linear equations while after linearizing the coupling is absent. The differences in the response magnitudes are attributed to the approximations introduced during the linearization of the non-linear model.

Analysis of both models reveals that their responses show unbounded divergent behaviour over time. It is evident that the system fails to return to equilibrium after a command input is applied, indicating that both plants are inherently unstable. Moreover, the instability of the uncontrolled plants demonstrates that they cannot meet the expected performance specifications of the system. This clearly highlights the necessity of implementing a controller to stabilize the system and ensure that it quickly recovers from destabilizing events. Without a controller, the system would remain unstable and incapable of achieving and sustaining the stable hover in challenging environments, particularly during high-rise building inspections. The controller can be made unnecessary by changing the drone parameters until they meet performance specifications and make the drone stable, but this approach will result in impractical parameters that can never be achieved realistically hence the only option to control stability is the introduction of the controller.

The stability behaviour for non-linear model was evaluated based on the system's response analysis done in previous section. This approach was chosen because criteria used for linear stability behaviour evaluation were not feasible due to the complex dynamics of the non-linear model. The system is considered stable when, after bounded input is applied, the output remains bounded and ideally settles near an equilibrium point over time [6]. Looking at the time response for non-linear model in previous section, the output grows without bound in response to a bounded input. Essentially, the system lacks control to stabilize once disturbed. Instead of converging to steady state after bounded input, the system amplifies deviation, leading to uncontrolled growth in the outputs. This implies that the system does not meet BIBO (Bounded Input Bounded Output) criterion hence it is unstable.

5.3 Linear model stability behaviour

5.3.1 Zero-Pole Stability Analysis

The pole-zero techniques were used to determine the regions of stability using the transfer functions for all directional movement of the quadrotor. Each transfer function is presented in Table 1.

Table 5: Transfer function for elevation, roll, pitch, and yaw

Movement	General Form	Specific Form
Elevation	$TFE = \frac{1}{ms^2}$	$\frac{1}{0.506s^2}$
Roll	$TFR = \frac{1}{I_{XX}s^2}$	$\frac{1}{8.12 \times 10^{-5}s^2}$
Pitch	$TFP = \frac{1}{I_{YY}s^2}$	$\frac{1}{8.12 \times 10^{-5}s^2}$
Yaw	$TFY = \frac{1}{I_{ZZ}s^2}$	$\frac{1}{6.12 \times 10^{-5}s^2}$

For a transfer function, the standard form for zero-pole is given by the expression below:

$$G(s) = K \frac{(s - z_1)(s - z_2) \cdots (s - z_m)}{(s - p_1)(s - p_2) \cdots (s - p_n)} \quad (90)$$

where the numerator represents the zeros, which are the values of s that make the transfer function equal to zero, and the denominator represents the poles, which are the values of s that make the transfer function approach infinity.

For a quadrotor, the transfer functions are in the same standard form:

$$TF(s) = \frac{1}{as^2} \quad (91)$$

where a is a constant. The transfer function does not have zeros, and all transfer functions have double poles at:

$$as^2 = 0 \implies s = 0 \quad (92)$$

The graph for both directional movement of the drone of the poles are the same and are shown in the Figure below

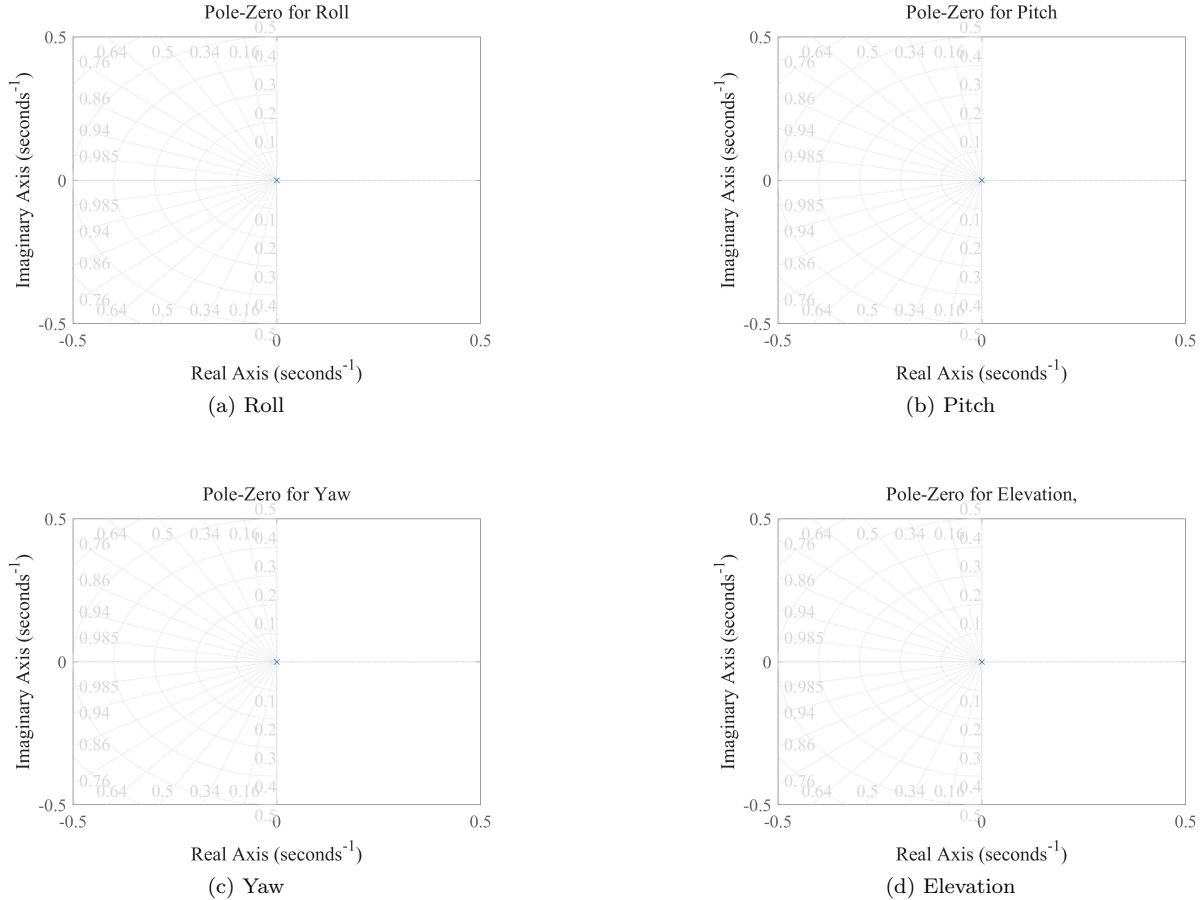


Figure 12: Pole Zero plots for quadrotor: (a) Roll, (b) Pitch, (c) Yaw, and (d) Elevation.

The poles of the system lie at the origin (zero), which means the quadrotor is marginally stable in all directions. This means the drone does not return to a steady position on its own. If the vertical thrust is increased, the drone will keep rising without reaching a stable height. If the yaw input is disturbed, the drone will keep spinning and will not be able to return to its original direction.

This shows that the system needs a controller to keep the drone stable. a control system must be added

to make sure the drone can stay balanced and return to its position after any disturbance.

5.4 Nyquist Stability Criterion

While the Zero-Pole plot method provided initial stability assessment, we verify the results using the Nyquist stability criterion. The standard transfer function for each axis is:

$$TF(s) = \frac{1}{as^2} \quad (93)$$

To apply the Nyquist method, we transform the transfer function to the frequency domain by substituting $s = i\omega$, where ω is the frequency in radians per second:

$$TF(i\omega) = \frac{1}{a(i\omega)^2} = -\frac{1}{a\omega^2} \quad (94)$$

The real and imaginary components of the transformed function are:

$$\text{Re}[TF(i\omega)] = -\frac{1}{a\omega^2} \quad (95)$$

$$\text{Im}[TF(i\omega)] = 0 \quad (96)$$

The Table 6 below shows the input values that were used to accurately obtain the Nyquist plot by varying the frequency from $-\infty$ to $+\infty$.

Table 6: Input values of frequencies to estimate the shape of Nyquist plot

	ω	Re	Im
1	0^+	$-\infty$	0
2	$-\infty$	0^-	0
3	$+\infty$	0^-	0

MATLAB was used to generate the Nyquist plots for each directional movement of the quadrotor. The plots are shown in Figure 4 below. All the Nyquist plots exhibit similar behaviour they lie entirely along the negative real axis of the complex plane. This occurs because the transfer functions contain only double poles at the origin with no zeros as shown during the zero-pole analysis and it resulted in a frequency response that is real and negative all the time. Since the Nyquist plots do not encircle the critical point $1+0j$, the system is classified as marginally stable. This means that while the system does not diverge, it also does not return to equilibrium without additional control.

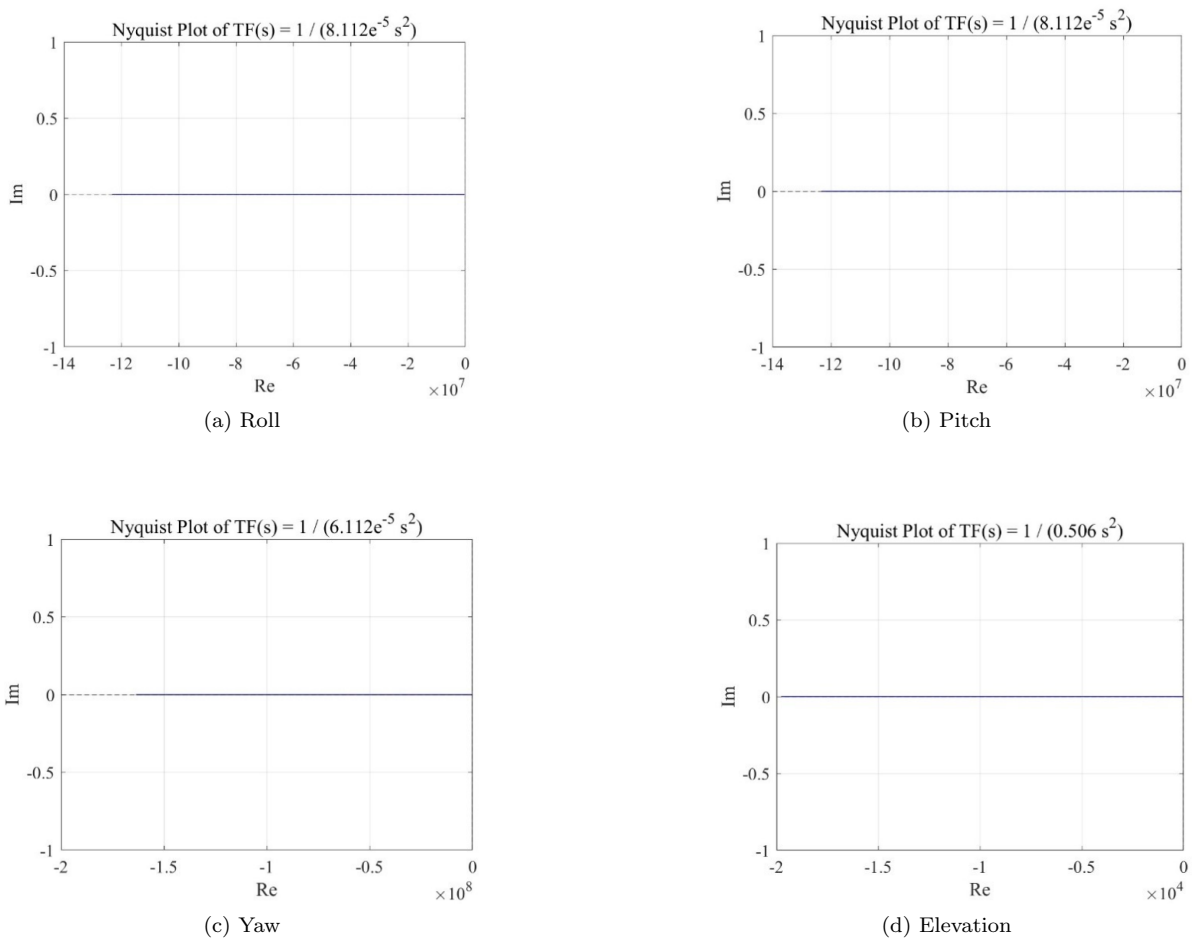


Figure 13: Nyquist plots for quadrotor dynamics: (a) Roll, (b) Pitch, (c) Yaw, and (d) Elevation.

5.4.1 Routh-Hurwitz Stability Criterion

The Routh-Hurwitz method is used for stability analysis. The general transfer function has the form:

$$TF(s) = \frac{1}{as^2} \quad (97)$$

where:

- $a = m$ for elevation
- $a = I_{yy} = I_{xx}$ for pitch and roll
- $a = I_{zz}$ for yaw

This gives the characteristic equation for all axes:

$$as^2 = 0 \quad (98)$$

In general polynomial form:

$$as^2 + 0s + 0 = 0 \quad (99)$$

Table 7: Routh-Hurwitz stability table

s^2	a	0
s^1	0	0
s^0	0	0

The system has poles only at the origin, indicating marginal stability. Both stability tests show that:

- The system doesn't grow unbounded
- It won't return to equilibrium after disturbance
- A control system is required for stabilization

5.4.2 Bode Plot Analysis

For a transfer function of the form:

$$TF(s) = \frac{1}{as^2} \quad (100)$$

The magnitude of the frequency response is:

$$|TF(i\omega)| = \left| \frac{1}{a(i\omega)^2} \right| = \left| \frac{1}{a\omega^2} \right| \quad (101)$$

The magnitude in decibels is:

$$M = 20 \log(|TF(i\omega)|) \quad (102)$$

$$= 20 \log \left(\frac{1}{a\omega^2} \right) \quad (103)$$

$$= 20 \log(1) - 20 \log(a\omega^2) \quad (104)$$

$$= 20 \log(1) - 40 \log(a\omega) \quad (105)$$

The phase calculation gives:

$$\theta = \tan^{-1} \left(\frac{\text{Im}}{\text{Re}} \right) = \tan^{-1} \left(\frac{0}{-1/a\omega^2} \right) = -180^\circ \quad (106)$$

Since the function only consists of the negative real part, this implies the phase is -180 degree.

Table 8: Bode functions from Transfer Function

Transfer Function	Magnitude M (dB)	Phase (Degree)
$TFE = \frac{1}{ms^2}$	$20 \log(1) - 40 \log(m\omega)$	-180
$TFR = \frac{1}{I_{XX}s^2}$	$20 \log(1) - 40 \log(I_{XX}\omega)$	-180
$TFP = \frac{1}{I_{YY}s^2}$	$20 \log(1) - 40 \log(I_{YY}\omega)$	-180
$TFY = \frac{1}{I_{ZZ}s^2}$	$20 \log(1) - 40 \log(I_{ZZ}\omega)$	-180

For each of the transfer functions in table 8, the Bode plots are shown in fig. 14 below.

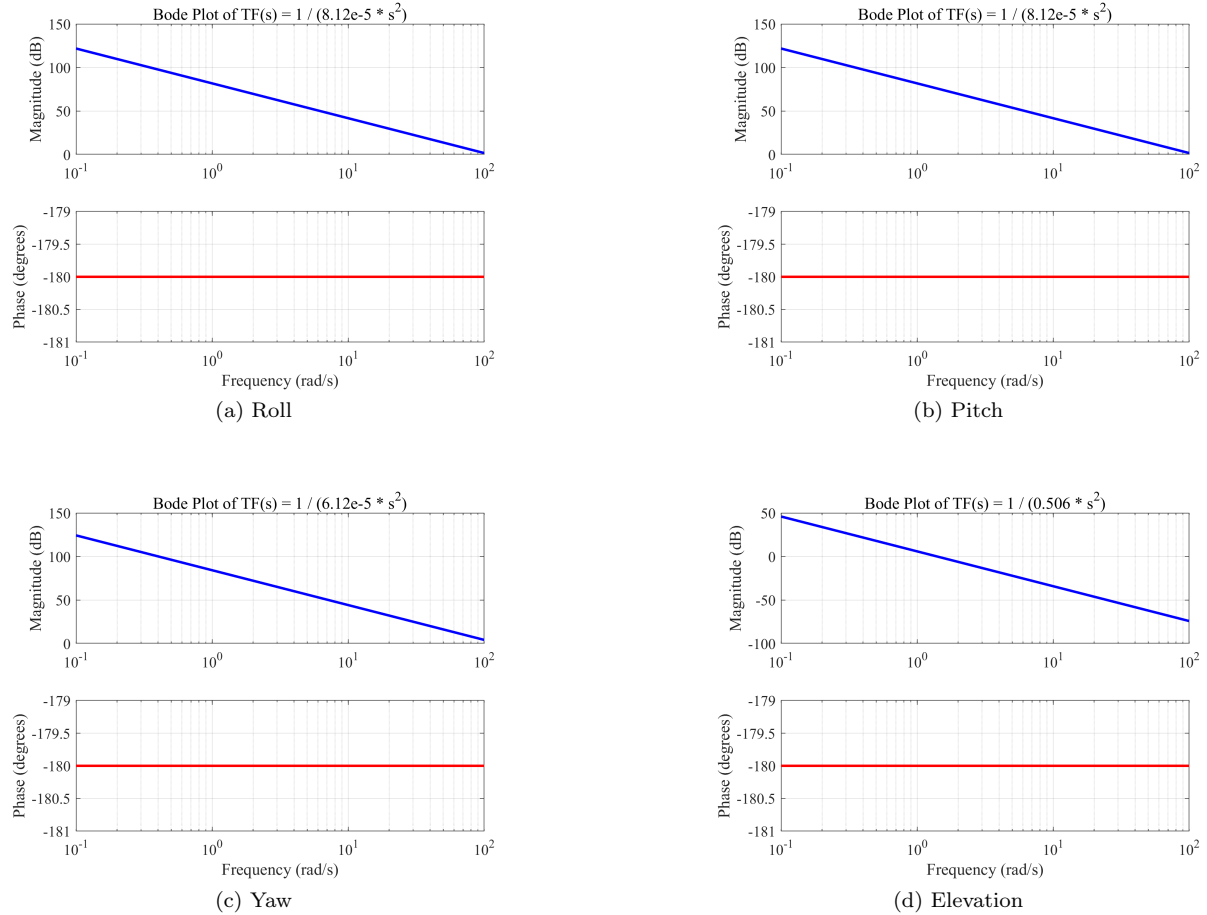


Figure 14: Bode plots for quadrotor dynamics: (a) Roll, (b) Pitch, (c) Yaw, and (d) Elevation.

6 Controller Design

6.1 PID controller

The system's response and stability analysis reveal that it is inherently unstable and cannot meet the desired performance specifications on its own. This is primarily due to the plant dynamics, which lack sufficient damping and responsiveness. Simply altering the physical parameters of the system to achieve stability is not practical, as it would require unrealistic changes that are not feasible in real-world scenarios. Therefore, to ensure system stability and achieve the desired performance specifications, a feedback controller is needed. The controller needs to actively monitors the system output and adjusts the control input in real-time to correct deviations and maintain the system's behaviour within acceptable limits. There are different types of controllers that can be implemented, and each is evaluated based on the system's performance specifications.

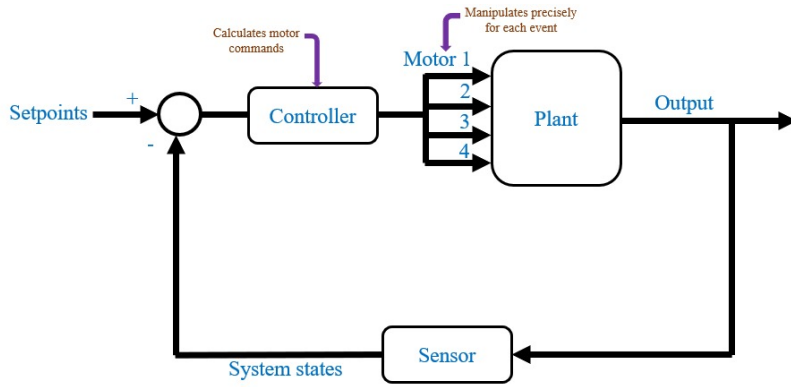


Figure 15: System Controller

To ensure that the drone meets the defined performance and stability objectives, the control strategies need to be analysed under defined objectives.

Freehand throw

In this scenario, the drone is manually thrown along the z-axis with an initial vertical velocity of 2 meters/second at a height of 5 meters to observe how the controller handles sudden changes in velocity without any external input forces or disturbances. The drone must counteract the initial momentum by adjusting motor thrust to stabilize at 5.6 meters according to the mission profile.

Freefall

In this scenario the drone is released (initial velocity = 0 m/s) at a height of 5 metres and must adjust motors to stabilize at 5.6 meters.

Upside-down

In this scenario, the drone starts in an inverted position. This is achieved by initializing the roll angle to 180 degrees. The earth-fixed reference frame remains stationary and does not rotate. This means the body's y-axis is in the opposite direction to the earth frame (i.e., 180° out of phase), while the x-axis remains aligned. The drone needs to rotate 180 degrees in roll to regain stability and hover at 5.6 meters

6.1.1 Different controller designs

Proportional Control

This control is directly proportional to the error signal(difference between the desired setpoint and the actual output). The control reduces the rise time and steady-state error but may not eliminate the error completely. The transfer function is given by:

$$\frac{Z}{Z_{\text{ref}}} = \frac{K_P}{as^2 + K_P}$$

The Routh-Hurwitz table for the characteristic equation $as^2 + K_P = 0$:

s^2	a	K_P
s^1	$2m$	0
s^0	K_P	

There is a sign change in the first column of the Routh-Hurwitz table, indicating the existence of a pole in the right-hand plane. The stability criterion is violated as not all roots of the characteristic equation lie in the left-hand plane. This is verified by the absence (zero coefficient) of the first-order term.

Integral control

-This control action is based on the integral of the past errors over time. The control eliminates steady-state error but can make the system slower and prone to instability.

The transfer function is given by:

$$\frac{Z}{Z_{\text{ref}}} = \frac{K_I}{as^3 + K_I}$$

The Routh-Hurwitz table for the characteristic equation $as^3 + K_I = 0$:

s^3	a	0	0
s^2	ϵ	K_I/a	
s^1	$-\infty$	0	
s^0	K_I/a		

There is a sign change in the first column of the Routh-Hurwitz table (from ϵ to $-\infty$), indicating the existence of at least one pole in the right-hand plane. The stability criterion is violated as not all roots of the characteristic equation lie in the left-hand plane. This instability is further evidenced by the absence of the first-order term (s^1 coefficient) in the characteristic equation.

Derivative control

-The control action is based on the derivative of the error. The action improves the system stability and reduces overshoot by anticipating the future errors.

The transfer function is given by:

$$\frac{Z}{Z_{\text{ref}}} = \frac{K_D}{as + K_D}$$

The closed-loop transfer function has a first-order characteristic equation. There is no sign change in the coefficients of the characteristic polynomial. The system is stable for $K_D > 0$ and unstable for $K_D \leq 0$.

However, derivative control cannot be used for second-order plant controllers as it cannot eliminate constant steady-state error.

Proportional plus Integral (PI) control

-Combines the proportional and integral control actions to improve response and steady-state error. The closed-loop transfer function is given by:

$$\frac{Z}{Z_{\text{ref}}} = \frac{K_P s + K_I}{as^3 + K_P s + K_I}$$

The Routh-Hurwitz table for the characteristic equation $as^3 + K_P s + K_I = 0$:

Order	Coefficient 1	Coefficient 2
s^3	a	K_P
s^2	$\lim_{\epsilon \rightarrow 0^+} \epsilon = 0^+$	K_I
s^1	$-\infty$	0
s^0	K_I	

There is a sign change in the first column of the routh Hurwitz table and therefore there exists a pole in the right-hand plane. The stability criterion is violated as not all roots of the characteristic equation lie on the left-hand plane. This is verified by the absence or zero coefficient of the second order term.

Proportional plus Derivative (PD) control

-Uses both proportional and derivative actions to balance response speed and stability but does not eliminate steady-state error

The closed-loop transfer function with PD control is given by:

$$\frac{Z}{Z_{\text{ref}}} = \frac{K_D s + K_P}{ms^2 + K_D s + K_P}$$

The characteristic equation is:

$$ms^2 + K_D s + K_P = 0$$

Order	Coefficient 1	Coefficient 2
s^2	a	K_P
s^1	$K_D - K_p$	0
s^0	K_P	

The closed loop transfer function has a characteristic equation of second order. There is no sign change in the coefficients of the characteristic polynomial. There is also no change in the first row of the routh Hurwitz hence the system is stable and needs to be evaluated.

All State Variables Over Time

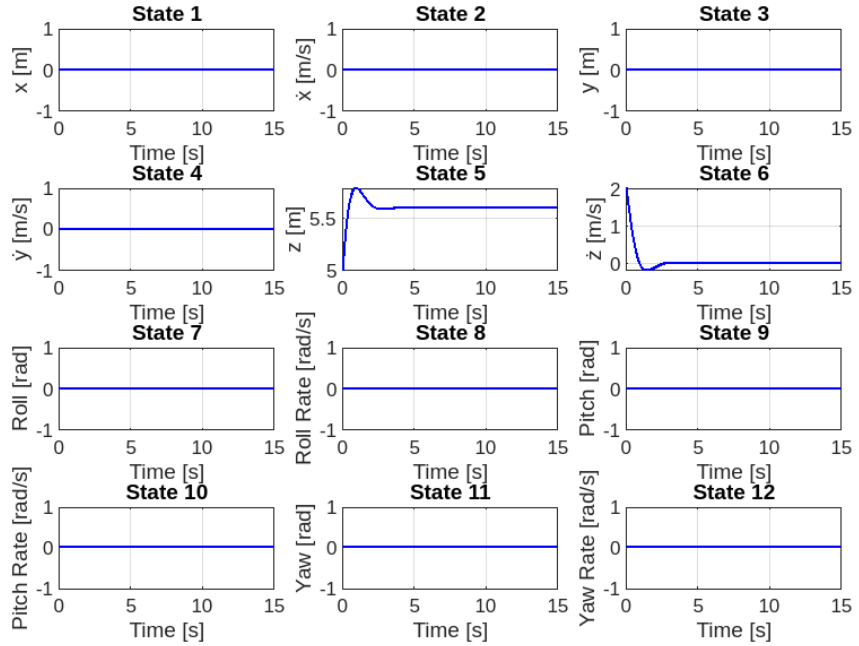


Figure 16: PD Freehand throw control

From Figure 16, when the initial z-velocity is applied, the system responds in both the z-position and z-velocity. Initially, the drone is at 5 meters. When the velocity is applied, the position increases over time, while the velocity decreases and eventually stabilizes around zero. The position stabilizes at around 5.6 meters. Both position and velocity reach steady state within the specified time of 7 seconds, and all other performance specifications, such as peak time and maximum overshoot, are also met. This indicates that the controller is successful for this event.

All State Variables Over Time

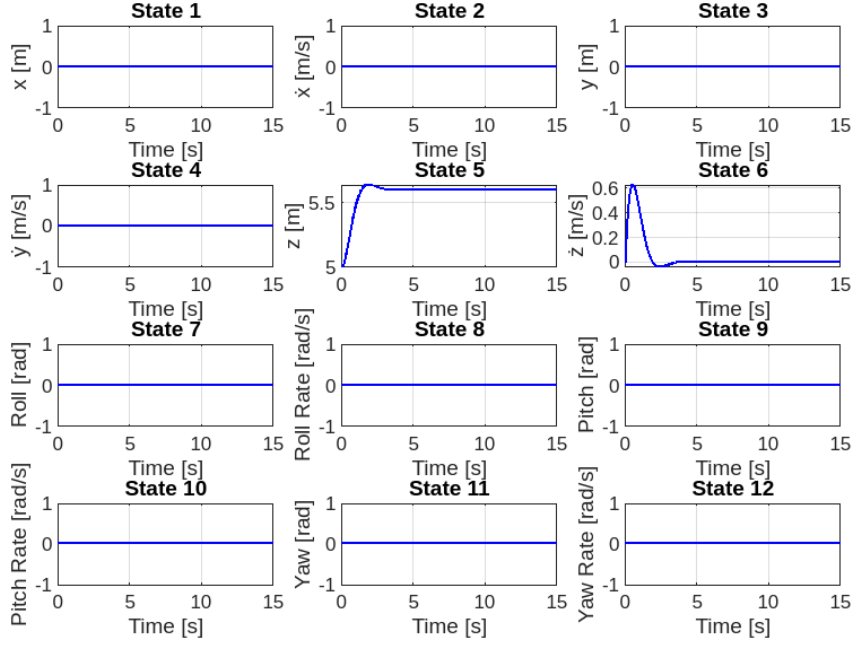


Figure 17: PD Free fall control

From the figures when the drone is released system responds in both the z-position and z-velocity. Initially, the drone is at 5 meters, when the drone is released, it gains the velocity until it reaches maximum then the motor thrust starts to overpower the freefall velocity until it reaches hover mode where it stabilizes and does not change the altitude. Both position and velocity reach steady state within the specified time of 7 seconds, and all other performance specifications, such as peak time and maximum overshoot, are also met. This indicates that the controller is successful for this event.

All State Variables Over Time

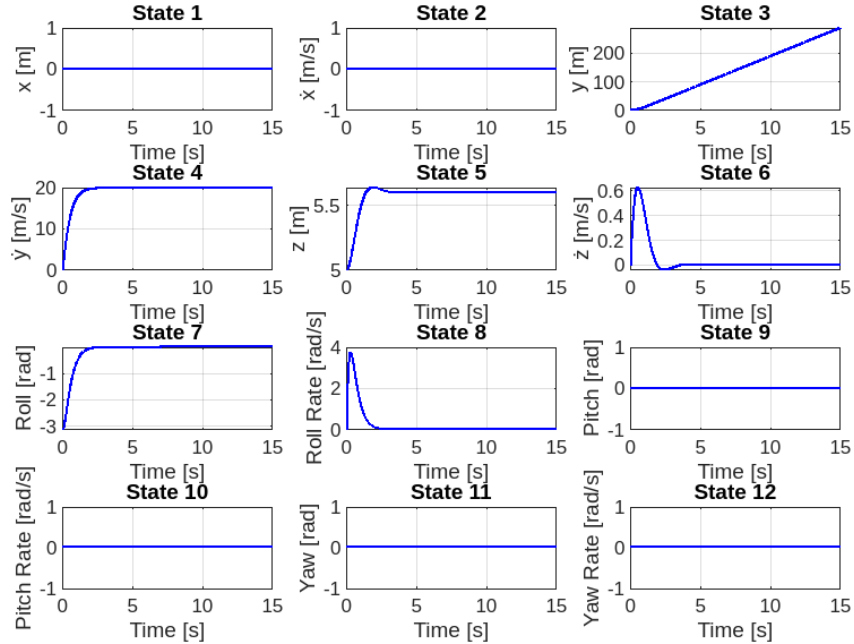


Figure 18: PD Upside down control

In the figure, when the drone is initially given a roll angle of 180 degrees and left to respond, six states are being monitored: the y-position and its velocity, the z-position and its velocity, and the roll angle with its roll rate. Starting with the roll angle and roll rate, the drone initially at -180 degrees then moves to 0 degrees where it reaches hover mode. This process occurs within a specified settling time. Similarly, the roll rate overshoots its maximum value before eventually stabilizing to zero, which indicates that the controller is stable for both the roll angle and roll rate. Looking at the z-position and velocity, the position gradually increases over time, overshooting the target before settling at the setpoint. Meanwhile, the velocity rises to a maximum value before decreasing to zero, achieving hover mode and stabilizing. This behaviour implies that the controller is stable for both the z-position and velocity.

However, for the y-position and velocity, the position continues to diverge while the velocity converges. This indicates that the controller is unable to stabilize the y-position, meaning another control strategy needs to be evaluated, as the current one does not meet the specifications for stable y-position control

Proportional + Integral+Derivative (PID) control:

Proportional + Integral+Derivative (PID) control Uses both proportional, integral and derivative actions to Balances fast response, minimal overshoot, and zero steady-state error. Requires careful tuning

$$\frac{Z}{Z_{\text{ref}}} = \frac{K_D s^2 + K_P s + K_I}{as^3 + K_D s^2 + K_P s + K_I}$$

$$\begin{array}{c|ccc} s^3 & a & K_P & 0 \\ s^2 & K_D & K_I & 0 \\ s^1 & \frac{K_D K_P - K_I a}{K_D} & 0 & 0 \\ s^0 & K_I & & \end{array}$$

The closed loop transfer function has a characteristic equation of third order. There is no sign change in the coefficients of the characteristic polynomial. There is also no change in the first row of the Routh-Hurwitz hence the system is stable and needs to be evaluated.

All State Variables Over Time

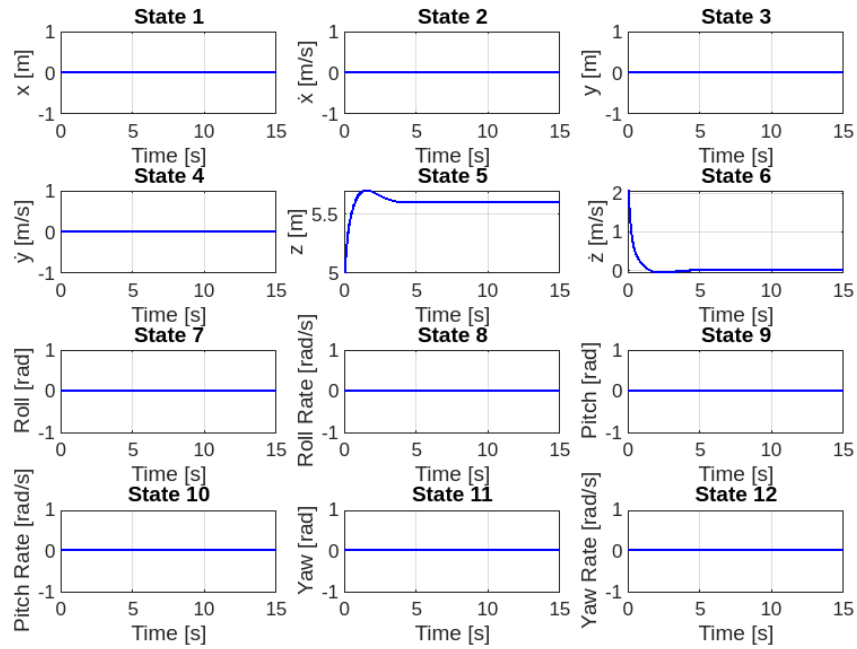


Figure 19: PID Freehand throw control

All State Variables Over Time

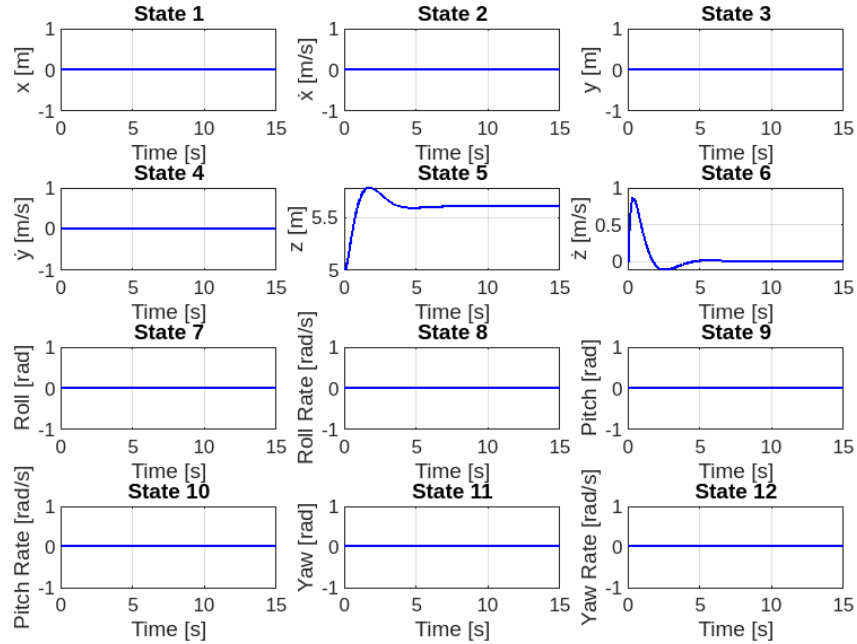


Figure 20: PID Free Fall control

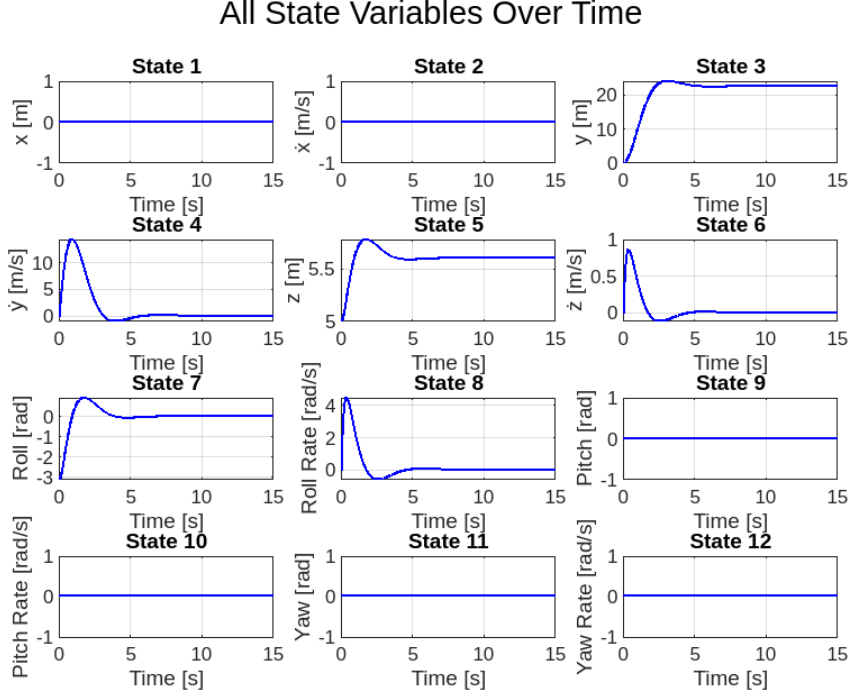


Figure 21: PID Upside down control

When the PID controller is implemented, the system's response is like the PD controller but with improved performance specifications, particularly in stabilizing the y-position. In the upside-down case, the PD controller failed to stabilize the y-position, causing it to diverge. However, with the addition of the integral term in the PID controller, the system was able to correct this drift over time, leading to better overall stabilization of the y-position. The integral action continuously accumulated and corrected the error, effectively addressing the steady-state error that the PD controller could not handle.

As a result, the PID controller not only maintained stability in the y-position but also improved the robustness of the system under more complex dynamics. This improvement indicates that the PID controller is better suited for nonlinear plant, as it can handle the additional complexities and uncertainties that typically arise in such systems, making it the preferred choice over PD controller when dealing with nonlinear dynamics.

6.1.2 PID tuning

The Proportional-Integral-Derivative (PID) controller is essential for quadrotor stability and precision control. PID tuning involves carefully adjusting three gain parameters: the proportional gain (K_p) that responds to immediate position errors, the integral gain (K_i) that eliminates accumulated steady-state errors, and the derivative gain (K_d) that anticipates and dampens future oscillations. This tuning process seeks optimal parameters that satisfy the control law:

$$u(t) = K_p e(t) + K_i \int_0^t e(\tau) d\tau + K_d \frac{de(t)}{dt} \quad (107)$$

where $u(t)$ represents the control output and $e(t)$ denotes the error between desired and actual states.

6.2 Rationale for Quadrotor Implementation

Quadrotors fundamentally require PID control due to their inherent instability and complex dynamics. The controller must simultaneously regulate four degrees of freedom (roll, pitch, yaw, and altitude)

while compensating for external disturbances. The proportional term provides immediate corrective action when the quadrotor deviates from its desired orientation or position. The integral term gradually eliminates persistent errors caused by factors like uneven weight distribution or constant wind pressure. The derivative term critically dampens the system's natural oscillatory tendencies, particularly important during aggressive maneuvers or when carrying inspection payloads.

For building inspection applications, PID controllers offer distinct advantages. They maintain position accuracy within ± 2 cm during hover, which is crucial for obtaining clear structural imagery. The derivative component minimizes vibration-induced blur in captured photos and videos, while the integral action compensates for battery drain-induced thrust variations during prolonged flights. Tuning typically begins with Ziegler-Nichols methods to establish baseline gains, followed by manual refinement to achieve response times under 0.5 seconds for disturbance rejection - a requirement when operating near buildings with unpredictable wind patterns. This combination of rapid response and steady-state precision makes PID control the preferred approach for commercial inspection drones.

6.2.1 System Setup

The plant is modeled as a second-order integrator:

$$G(s) = \frac{1}{ms^2} \quad (108)$$

6.2.2 Desired Characteristic Equation

Given design parameters $\zeta = 0.635$ and $\omega_n = 1.356$, we derive:

$$s^2 + 2\zeta\omega_n s + \omega_n^2 = s^2 + 1.721s + 1.839 \quad (109)$$

Augmented with an additional pole $(s + a)$:

$$(s^2 + 1.721s + 1.839)(s + a) = s^3 + (1.721 + a)s^2 + (1.839 + 1.721a)s + 1.839a \quad (110)$$

6.2.3 Controller Structure

The PID controller transfer function:

$$C(s) = K_d s^2 + K_p s + K_i \quad (111)$$

6.2.4 Closed-Loop Analysis

Open-loop transfer function:

$$L(s) = \frac{K_d s^2 + K_p s + K_i}{ms^2} \quad (112)$$

6.2.5 Closed-loop characteristic equation

$$1 + L(s) = 0 \Rightarrow ms^3 + K_d s^2 + K_p s + K_i = 0 \quad (113)$$

6.2.6 Gain Calculation

Equating coefficients between (113) and (110):

$$K_d = m(1.721 + a) \quad (114)$$

$$K_p = m(1.839 + 1.721a) \quad (115)$$

$$K_i = m(1.839a) \quad (116)$$

6.2.7 Final PID Gains

The symbolic PID gains in terms of mass m and pole location a :

- Derivative gain: $K_d = m(1.721 + a)$
- Proportional gain: $K_p = m(1.839 + 1.721a)$
- Integral gain: $K_i = m(1.839a)$

Table 9: Controller Gains for Various Third Pole Locations

Third Pole $s = -b$	K_p	K_i	K_d
$S = -1$	$m(1.839 + 1.721a)$	$m(1.839a)$	$m(1.721 + a)$
$S = -3$	$m(4.721)$	$m(7.002)$	$m(5.517)$
$S = -5$	$m(6.721)$	$m(10.444)$	$m(9.195)$
$S = -10$	$m(11.721)$	$m(19.049)$	$m(18.39)$

Table 10: Final Summary Table of PID Gains (Analytical)

Parameter	a	K_d	K_p	K_i
mass m (0.506)	1	$0.506 \times 2.721 = 1.377$	$0.506 \times 3.56 = 1.800$	$0.506 \times 1.839 = 0.931$
	3	2.387	3.543	2.793
	5	3.403	5.283	4.654
	10	5.936	9.635	9.295
$8.12e-5$	1	2.211e-4	2.890e-4	1.494e-4
	3	3.832e-4	5.684e-4	4.480e-4
	5	5.460e-4	8.482e-4	7.472e-4
	10	9.520e-4	1.548e-3	1.494e-3
$6.12e-5$	1	1.667e-4	2.179e-4	1.126e-4
	3	2.888e-4	4.286e-4	3.374e-4
	5	4.112e-4	6.390e-4	5.624e-4
	10	7.172e-4	1.166e-3	1.126e-3

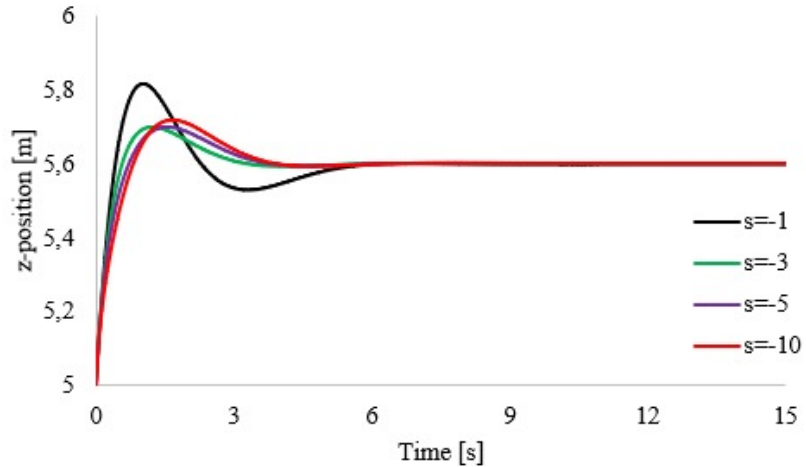


Figure 22: Tuned PID response

After careful tuning, the final gains have been set to $S = -5$. These gains were chosen because they result in the smallest overshoot and settling time, while also allowing the system to reach steady state quickly important for the mission.

6.2.8 PID controller evaluation

The controller to be used for the system is PID. This control action is implemented to evaluate how the non-linear system will respond, and results are presented below.

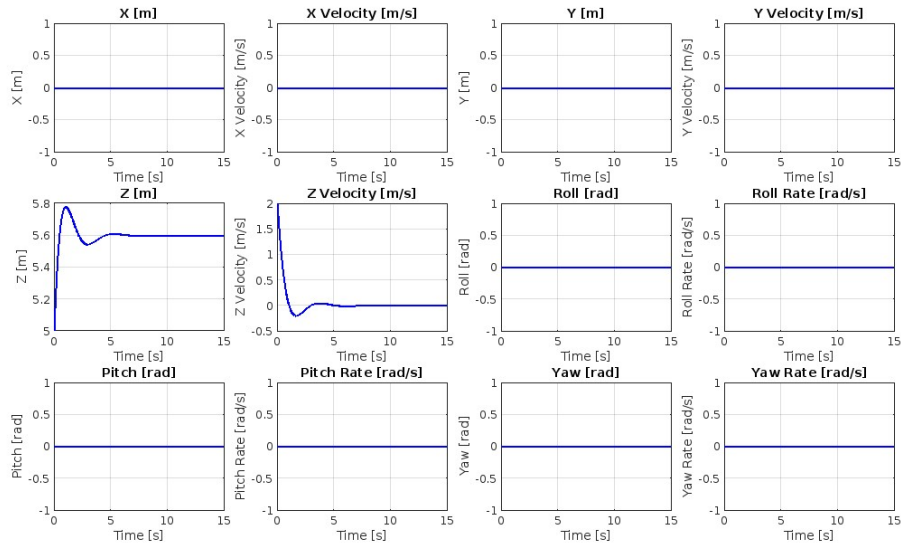


Figure 23: Non linear Free hand throw PID controller output

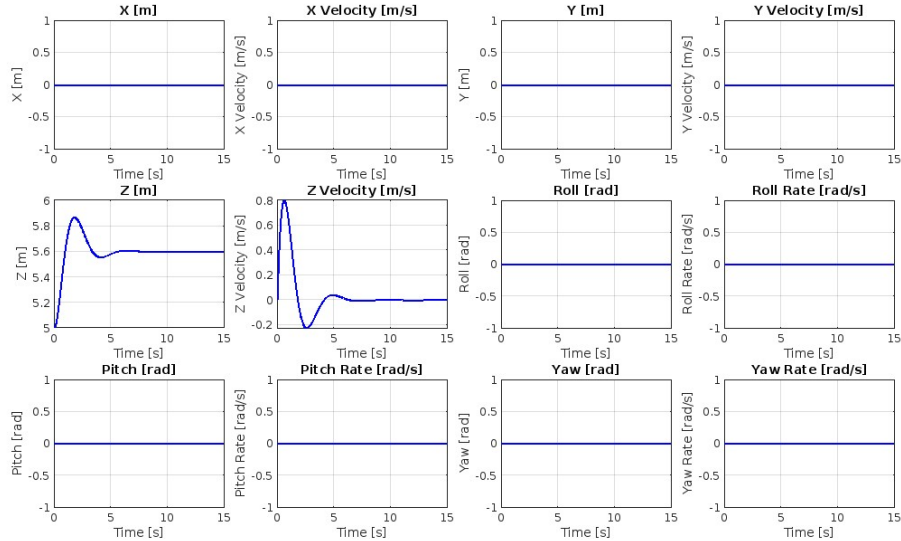


Figure 24: Non linear Free fall PID controller output

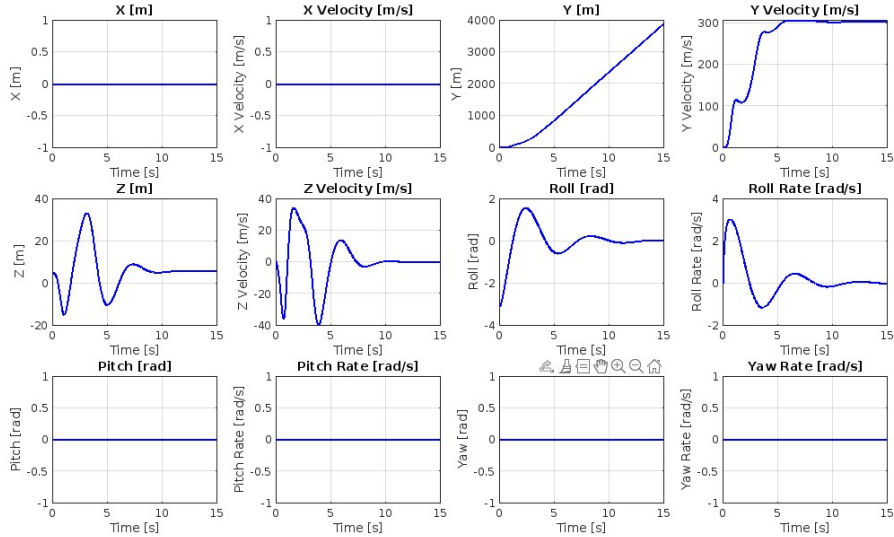


Figure 25: Non linear Upside down PID controller output

Comparing the responses of the controlled non-linear plant with the linear plant, the graphs for both the freehand throw and free fall events show matching behaviour. This indicates that the gains selected for the linear plant can also effectively control the non-linear plant. After implementing the PID controller, the non-linear plant demonstrates stable behaviour and meets the desired performance specifications, suggesting that the PID control is successful for these events.

However, when comparing the responses for the upside-down configuration event, the non-linear plant exhibits significant oscillations in vertical position, velocity, roll, and roll rate, with a settling time exceeding 7 seconds. Additionally, the y-position graph continues to diverge, and the velocity stabilizes at very high values, indicating that the chosen gains are not robust enough for this scenario.

6.3 Root-locus technique

6.3.1 Concept

Root locus is a graphical control technique that tracks the closed-loop transfer function poles as a parameter varies. The “locus” refers to the trajectory of these poles. Similar to Nyquist plots, root locus can determine:

- Absolute stability ranges
- Relative stability characteristics
- Parameter sensitivity

6.3.2 Controller Design Methodology

When combined with PID design:

- Maintains time-domain specifications
- Verifies controller gains
- Uses standard form: $1 + \frac{KN(s)}{D(s)} = 0$

Design objectives:

1. Formulate problem in root locus form
2. Plot and analyze using MATLAB
3. Determine gains at design points ($\zeta, \omega_n, \%OS$)
4. Verify parameters
5. Calculate minimum time constant
6. Validate stability and transient response
7. Ensure continuous stability
8. Identify tuning actions if needed

6.3.3 Root locus solution

The closed loop control system transfer is $T(s) = \frac{G(s)}{1 + G(s)H(s)}$; Where $G(s)$ is the plant transfer function and $H(s)$ is the negative feedback element dynamics.

The closed loop characteristic equation is therefore of the form $1 + G(s)H(s) = 0$

$$H(s) = 1$$

$$\text{Plant transfer function: } G_p(s) = \frac{1}{ms^2}$$

Integral control

$$\text{Integral controller transfer function } G_c(s) = \frac{1}{s}$$

$$\text{Input command transfer function: } R(s) = \frac{1}{s}$$

$$\text{Root locus technique form: } \frac{K}{ms^3} = 0$$

$$\text{Which is } ms^3 + K = 0 \rightarrow 1 + \frac{K(1/m)}{s^3}$$

Table Routh Hurwitz criterion for integral control for altitude.

s^3	m	0
s^2	$\lim_{\epsilon \rightarrow 0^+} \epsilon = +0$	K
s^1	$\lim_{\epsilon \rightarrow 0^+} \frac{-mK}{\epsilon} = \infty$	0
s^0	$-\left(\frac{-(mK^2)}{\epsilon}\right) \cdot \left(\frac{-\epsilon}{mK}\right) = -K$	

Values of the gain (K) for which the system is always stable: The system is stable for $K < 0$ such that 3rd row is positive and similarly 4th row.

$$K = -(ms^3)$$

$$\frac{dK}{ds} = -(3ms^2) = 0$$

The solutions are $s_{1,2} = 0$, because m is non-zero. This is the breakaway points.

The time constant τ cannot be less than infinity. And therefore, the system is expected to have all roots at the origin with this controller. For a second order system, independent integral control did have a nonzero probability of a destabilized system and thus this is not a surprise.

The altitude, pitch and roll control have the same form of the closed transfer function. The formulation and solution will be identical.

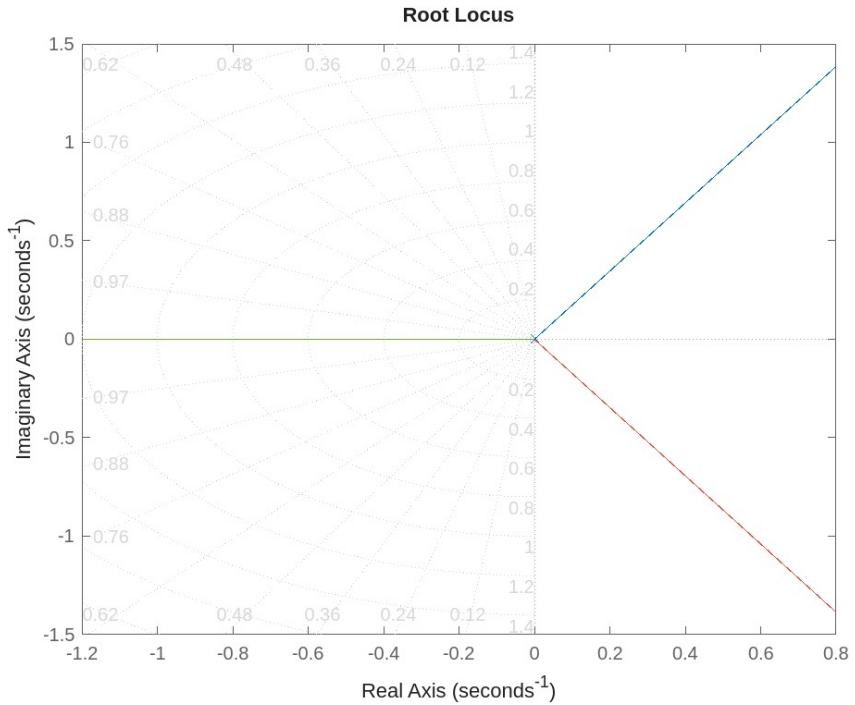


Figure 26: Root locus plots of the integral control of the altitude controller.

Figure shows the altitude controller root locus. All the poles are at the origin and therefore the system is unstable. The 3rd order system means all the poles are labelled ‘1’ and therefore the locus exists to the left of the origin on the real axis. There are no zeros ($Z=0$) and therefore the locus terminates at infinity along the three straight line asymptotes. The graphs shows that the there is no time constant as the breakaway point is at the origin. The next to graphs are similar to this.

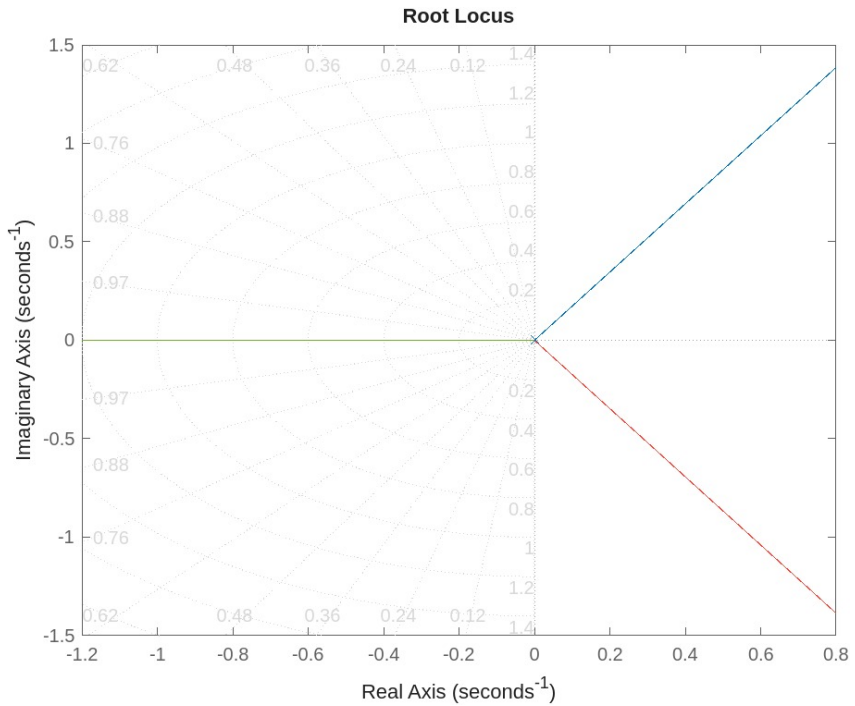


Figure 27: Root locus plots of the integral control of the pitch and/or roll controller.

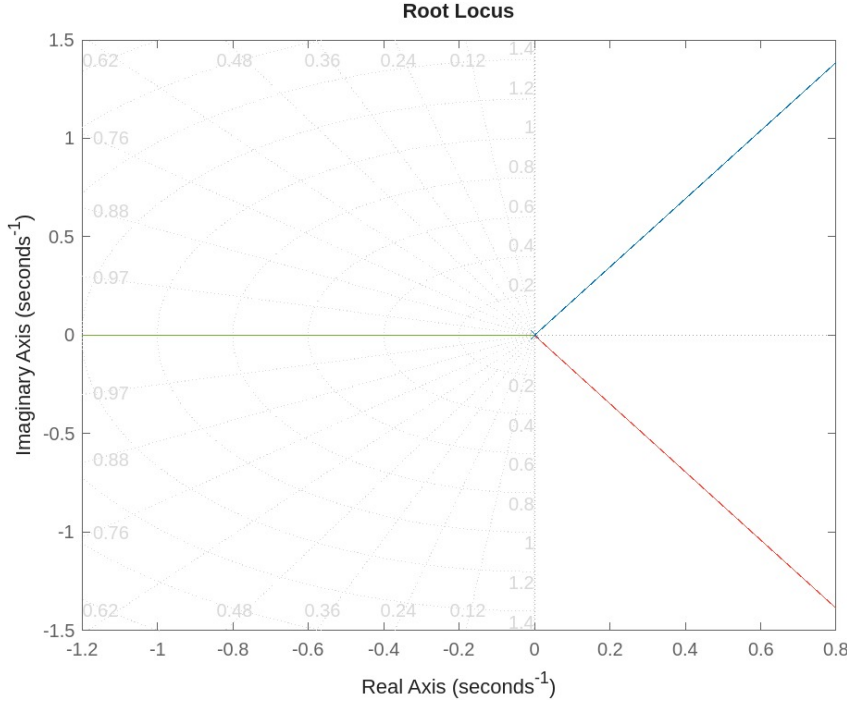


Figure 28: Root locus plots of the integral control of the yaw attitude controller.

Proportional derivative controller

Plant transfer function: $G_p(s) = \frac{1}{ms^2}$

First try PD control: $G_c(s) = K + K_d s$

Use root locus method to modify the PD controller so that the system is always stable.

Find smallest dominant time constant achievable with this design.

So now we have:

$$\frac{K + K_d s}{ms^2} = 0$$

which is:

$$ms^2 + K_d s + K = 0$$

Routh-Hurwitz criterion:

s^2	m	K
s^1	K_d	0
s^0	$-\frac{K_d K}{m}$	0

Therefore, for the system to be stable, $K_d > 0$ and $K > 0$.

$$K = -(ms^2 + K_d s + K)$$

$$\frac{dK}{ds} = -(2ms + K_d) = 0$$

The solutions are $s = -\frac{K_d}{2m}$, because m is non-zero.

The time constant cannot be less than $\tau = \frac{2m}{K_d}$.

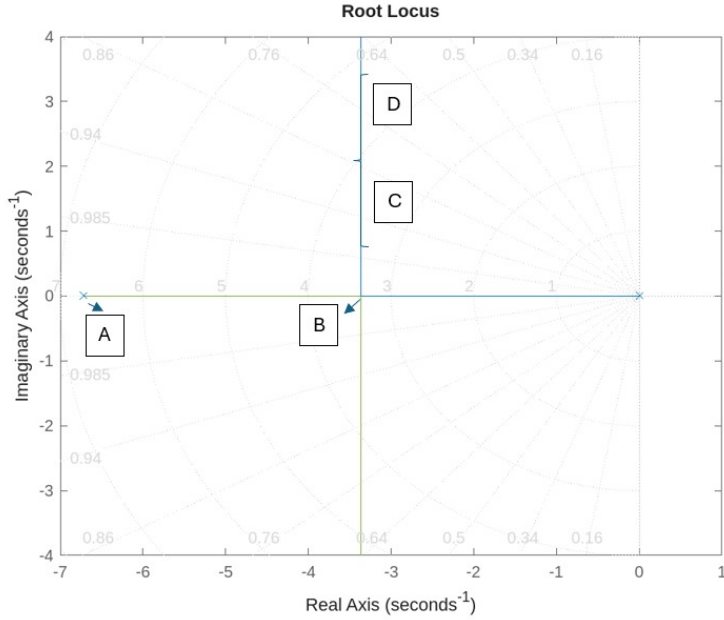


Figure 29: Root locus plot of proportional derivative controller applied for the altitude controller

The PD controller for altitude has a 2nd order characteristic polynomial. There are two roots with one at the origin and the other at A. Therefore, the locus exists between the origin and point A. If the gain value is greater than 0, the system is stable. The breakaway point is at B where the two roots depart real axis to infinity. This can be shown by the fact that gain increase along the vertical line at B. The PD gain varied variable is the proportional gain from the plant-preceeding PD controller.

PD Control Varies Proportional Control in K

Point	A	B	Arbitrary points on imaginary axis close to design point	Design point (OS 7.5%) ($\zeta = 0.645$) ($\omega_n = 1.356$)
Gain	0	5.71	15.1	13.3
Pole	-6.72	-3.36	-3.36+4.32i	-3.36+3.78i
Damping	1	1	0.614	0.6555
Overshoot %	0	0	8.68	6.55
Frequency (rad/s)	6.72	3.36	5.47	5.13

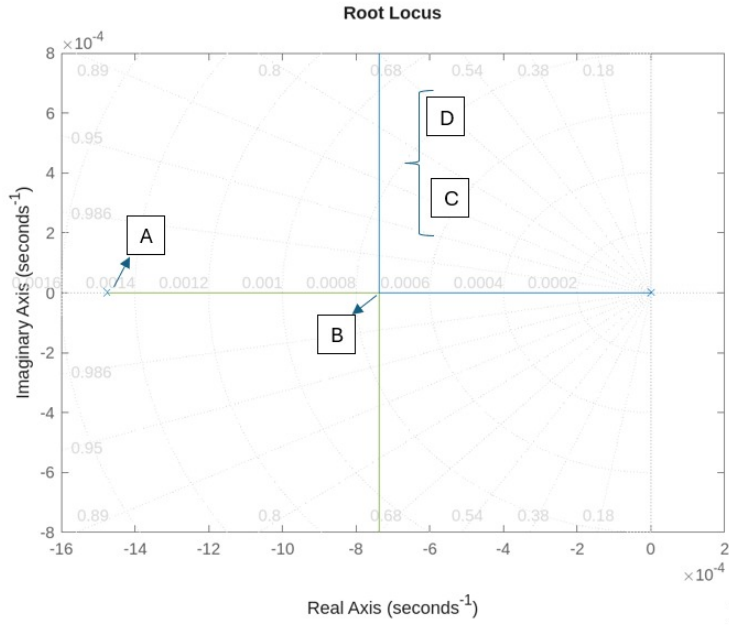


Figure 30: Root locus plot of proportional derivative controller applied for Roll/Pitch

Figure shows the root locus for the roll and/or pitch controller. The system is once again identical to the previous root locus with a stable system for $k = K_p > 0$. However, the gain margin has increased as the left most pole is at approximately -15 from approximately half that in the altitude controller. Roll and/or yaw is interestingly having larger relative stability than the altitude controller although they are both stable.

PD Control Varies Proportional Control in K

Point	A	B	Arbitrary points on imaginary axis close to design point	Design point (OS 7.5%) ($\zeta = 0.645$) ($\omega_n = 1.356$)
Gain	0	4.42×10^{-11}	1.03×10^{-10}	1.15×10^{-10}
Pole	-0.00148	-0.000738	-0.000738 +0.00086i	-0.000736 +0.000931i
Damping	1	1	0.651	0.621
Overshoot %	0	0	6.75	8.28
Frequency (rad/s)	0.00148	0.000738	0.00113	0.00119

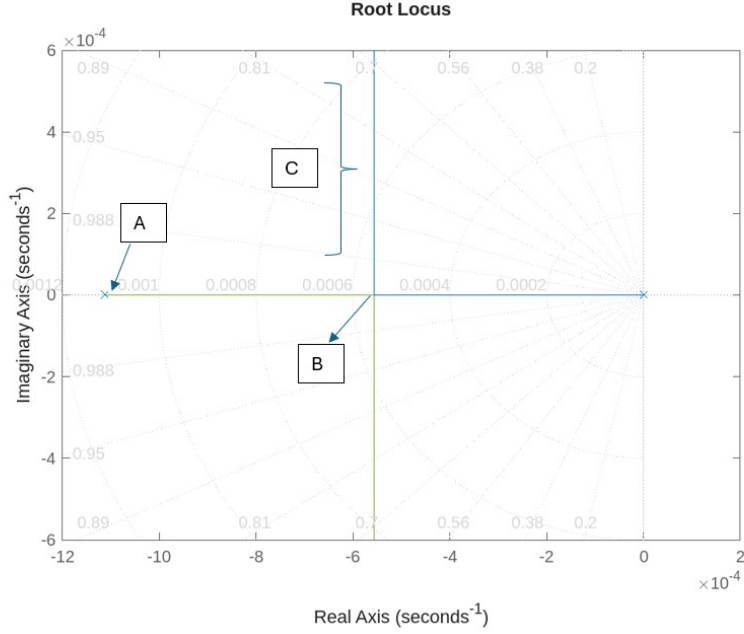


Figure 31: Root locus Integral control for yaw

Figure shows the root locus plot for the PD control for yaw controller. The yaw controller gain margin is approximately the same for the roll and/or yaw controller. Therefore, it can be concluded that this counterintuitively good. As long as the margin for attitude control is large, where we expect small damping.

Table 11: PD Control Varies Proportional Control in K

Point	A	B	Design Point (OS 7.5%, $\zeta = 0.645$, $\omega_n = 1.356$)
Gain	0	1.89×10^{-11}	4.91×10^{-11}
Pole (s)	-0.00111	-0.000556	$-0.000556 \pm 0.000702i$
Damping (ζ)	1	1	0.621
Overshoot (%)	0	0	8.28
Frequency (rad/s)	0.00111	0.000556	0.000895

6.3.4 PID Control Using Routh-Hurwitz

Plant transfer function: $G_p(s) = \frac{1}{ms^2}$

PID controller transfer function: $G_c(s) = K + \frac{K_I}{s} + K_d s$

Plant and controller in series:

$$P(s) = \frac{N(s)}{D(s)} = \frac{Ks + K_I + K_d s^2}{ms^3} = 0$$

Closed loop transfer function characteristic equation:

$$ms^3 + K_d s^2 + Ks + K_I = 0$$

Routh-Hurwitz table:

s^3	m	K
s^2	K_d	K_I
s^1	$\frac{-(mK_I - KK_d)}{K_d}$	0
s^0	$\frac{-(-K_I) \left(\frac{-(mK_I - KK_d)}{K_d} \right)}{\frac{-(mK_I - KK_d)}{K_d}} = K_I$	

Therefore, for the system to be stable:

$$\begin{aligned}
 K_I &> 0 \quad \text{and} \\
 \frac{-(mK_I - KK_d)}{K_d} &> 0 \\
 mK_I &> -K_d + KK_d \\
 mK_I &> K_d(K - 1)
 \end{aligned}$$

From the characteristic equation:

$$K_I = -(ms^3 + K_d s^2 + Ks)$$

$$\frac{dK}{ds} = -(3ms^2 + 2K_d s + K) = 0$$

The solutions are:

$$s_{1,2} = \frac{-(-2K_d) \pm \sqrt{4K_d^2 - 4(3m)(K)}}{2(3m)}, \quad \text{because } m \text{ is non-zero}$$

The time constant cannot be less than:

$$\tau = \frac{1}{\text{Re}(s_1)} \quad \text{or} \quad \frac{1}{\text{Re}(s_2)}$$

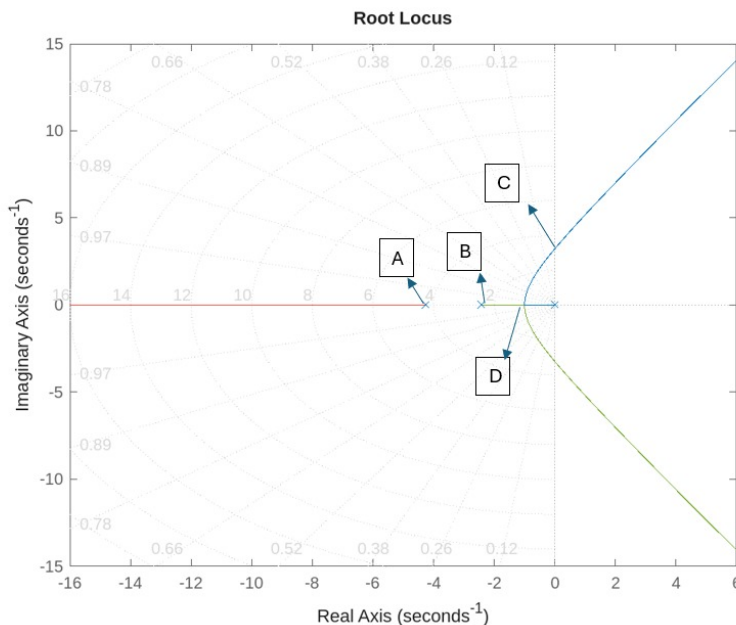


Figure 32: PID control root locus for altitude

Figure shows the loci for the altitude closed loop. When the standard form of root locus problem formulation is written, the variable parameter is a parameter $K=K_I$. Therefore, that means the other gains K_p and K_d are constant. This root serves two functions therefore, sensitivity to the integral gain and also gain values for which the system is stable proportionally. The characteristic polynomial is a 3rd order. The root locus exists on the real axis between the origin and point 2. The numerator of the transfer function is a second order and therefore there are two zeroes. The two loci must exist between the origin and the B towards each other and therefore point D is a breakaway point at which point the loci depart the real axis. The third root by definition must extend to infinity along the real axes. The stable is stable because all the roots are on the left-hand plane given that the gain is greater than 0 thus the loci do not start at the origin. The system becomes unstable at point labelled C and therefore giving the gain margin of approximately 36.1 which can be interpreted as relative stability.

Table 12: Root Locus Points for PID Altitude Control ($k_p = 5.28$, $k_I = 4.65$, $k_D = 3.4$)

Point	A	B	C	D	Design Vicinity (OS 7.5%, $\zeta = 0.645$, $\omega_n = 1.356$)	
Gain	0	0	36.1	2.38	4.17	4.17
Pole (s)	-4.28	-2.44	$0.115 + 3.25i$	-1.04	$-0.886 + 0.939i$	$-0.848 + 1.09i$
Damping (ζ)	1	1	-0.00353	1	0.686	0.613
Overshoot (%)	0	0	101	0	5.16	8.76
Freq. (rad/s)	4.28	2.44	3.25	1.04	1.29	1.38

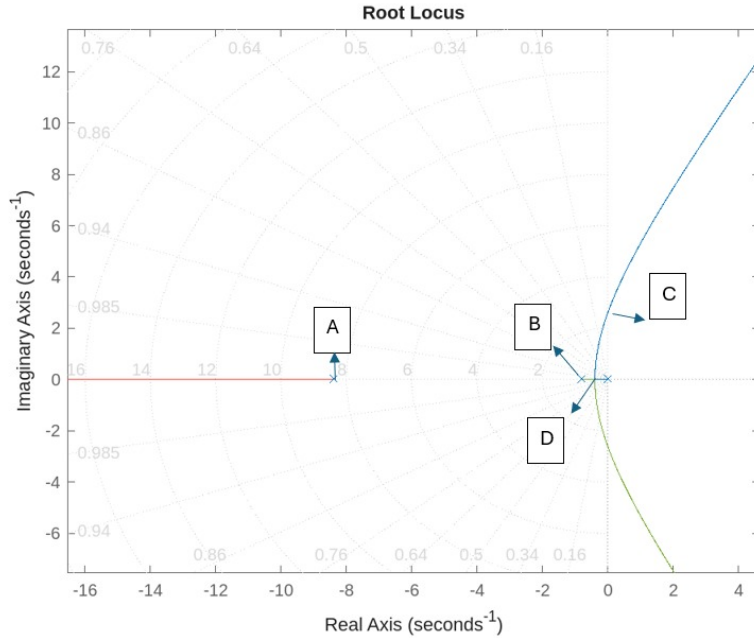


Figure 33: PID for Roll/Pitch

Figure similarly shows the root locus for the identical PID controllers for pitch attitude and roll attitude. The root locus is the same form as the root locus of altitude in terms of where the root locus exists by labels “A, B, C,D.” However more importantly, the gain margin is very very low indicating that there is low relative stability at magnitudes of 0.00496. This is extremely low considering the last controller and therefore it would be wise to retune the controller PIDs albeit the damping and natural frequency are within design specifications.

Table 13: Yaw/Roll Controller with PID Gains ($k_p = 0.000546$, $k_I = 0.000848$, $k_D = 0.00747$)

Point	A	B	C	D	Design Vicinity (OS 7.5%, $\zeta = 0.645$, $\omega_n = 1.356$)	
Gain	0.000306	0	0.00496	0.000104	0.000246	0.0002
Pole (s)	-8.46	-0.801	$-0.00445 + 2.58i$	$-0.39 + 1.49 \times 10^{-8}i$	$-0.377 + 0.4671i$	$-0.381 + 0.382i$
Damping (ζ)	1	1	0.00173	1	0.628	0.706
Overshoot (%)	0	0	99.5	0	7.95	4.35
Freq. (rad/s)	8.46	0.801	2.58	0.39	0.6	0.54

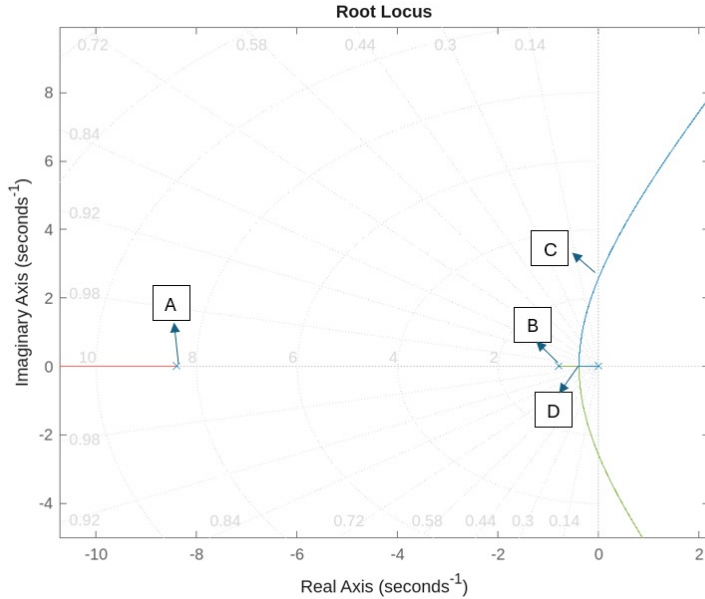


Figure 34: PID controller root locus for the yaw controller.

Table 14: Yaw Controller Root Locus with PID Gains ($k_p = 0.000411$, $k_I = 0.000639$, $k_D = 0.00563$)

Point	A	B	C	D	Design Vicinity (OS 7.5%, $\zeta = 0.645$, $\omega_n = 1.356$)	
Gain	0	0	0.00373	7.83×10^{-5}	0.000186	0.00015
Pole (s)	-8.4	-0.801	$-0.00441 + 2.58i$	$-0.39 + 1.76 \times 10^{-8}i$	$-0.376 + 0.4671i$	$-0.381 + 0.382i$
Damping (ζ)	1	1	0.00171	1	0.627	0.706
Overshoot (%)	0	0	99.5	0	7.96	4.36
Freq. (rad/s)	8.4	0.801	2.58	0.39	0.6	0.539

Figure 34 shows the root locus when PID is implemented for the yaw controller. The same form of loci paths and stability can be said for this root locus i.e. all poles are in the left hand side plane. The major interest is the gain margin or relative stability. At point C (imaginary axis intercept), the gain is still the order of 0.00373 which is slightly lower than for pitch and/or roll attitude controller.

6.3.5 Less Dominant Root Concept

This section evaluates the dominant root concept and verifies the predictions from the root locus plot against simulation observations. For a characteristic polynomial of order 2 or more, there may exist a dominant root which influences the system after the transient response dies out. The dominant root explores the largest time constant while the root locus explores the minimum, which serves as an indicator

of the system's transient response.

Table 15: Minimum Time Constant for Different Controllers

Root Locus Controller	Controller	PID
$N(s)/D(s)$ therefore $D(s)$		$s = [0 \ 1/m]$
$t = [1 \ k_d/m \ k_p/m \ 0]$		

Table 16: Breakaway Points and Minimum Time Constants

Parameter	Controller Type	Value
Breakaway point	Yaw control	$-0.39 + 1.76 \times 10^{-8}i$
	Pitch &/Roll	$-0.39 + 1.49 \times 10^{-8}i$
	Altitude	-1.04
Minimum time constant $\tau_{min} = -1/\text{breakaway}$	Yaw control	2.56
	Pitch &/Roll	2.56
	Altitude	0.96

The table shows that the minimum time constant for the controllers is 2.56 seconds, resulting in a settling time of approximately 10.24 seconds (4τ). For the minimum time constant of 0.96 seconds, the settling time is approximately 3.84 seconds. The former settling time is just outside the design specifications of 10 seconds, which can be attributed to the approximation of complex breakaway points that should ideally be real negative numbers. Near the real axis, the root parameters change rapidly, leading to errors in approximating the minimum time constant.

As evidence, the purely real breakaway point at -1.04 yields a time constant minimum of 0.96 seconds, which matches simulation data showing the quadcopter's altitude settling time of approximately 0.4 seconds. MATLAB's discrete root locus analysis contributes to these approximations, as it cannot select the loci as a perfect continuum. Overall, the design meets the specifications for stability, transient response, and steady-state error, with the root locus method corroborating the PID controller performance.

7 Discussion

The aim of the project was to design a controller for a drone system that is going to be used for high rise building inspection. The system was designed with a goal of meeting the specified specifications in the specified time-domain and frequency domain. The time domain was used to analyse the responds of the system over time while the frequency domain was used for system behaviour and stability. The drone modelled needs to maintain stability during hover and be capable of quickly recovering from destabilizing events such as freehand throw, freefall and upside-down orientation.

The system was modelled and was then linearized to simplify the analysis. Both non-linear and linear models were analysed for response using different inputs. The responses for both models showed high correlation meaning that the linear model can reliably represents the non-linear model under the defined conditions. This validation allowed the plant to be further analysed using linear model. The plant was analysed for stability and the criteria that were used are zero-pole, nyquist, Routh-Horwitz, bode plot. These criteria all implied that the system is unstable, and it was concluded that the linear plant is unstable. For non-linear plant the time responses were used, and they showed that when the bounded input is applied the bounded output is not obtain which does not meet the BIBO criterion and was concluded that the non-linear plant is also not stable. After the stability analyses revealed that the plants are unstable, the controller had to be implemented.

The root locus technique was applied for closed loop, and it improved the model to meet the deaired performance specification and the system became more stable. The controller was also implemented to actively monitor the system output and adjust the control input in real-time to correct deviations and maintain the system's behaviour within acceptable limits. Different controllers were evaluated and after analyses it was decided to use PID as it improved the system to meet the desired performance specifications for all states. The final performance specifications after PID implementation are peak time less than 3 seconds, maximum overshoot less than 7.5

8 Conclusion

Key findings from the project:

- The linear model proved reliable for analysis, effectively replacing the non-linear model
- Stability criteria confirmed uncontrolled plants are unstable, necessitating a controller
- The PID controller demonstrated robustness against defined destabilizing events
- The implemented controller successfully met all performance specifications

References

- [1] GarudaUAV, “GarudaUAV Official Website.” [Online]. Available: <https://garudauav.com/>. [Accessed May 20, 2025].
- [2] MepsKing, “What Are the Parts of FPV Drone,” 2023. [Online]. Available: <https://www.mepsking.shop/blog/what-are-the-parts-of-fpv-drone.html>. [Accessed: 21 May 2025].
- [3] W. Selby, “Quadrotor System Modeling - Non-linear Equations of Motion,” 2020. [Online]. Available: <https://wilselby.com/research/arducopter/modeling/>. [Accessed May 20, 2025].
- [4] W. Selby, “Quadrotor Control System Design - Position, Attitude, and Motor Control,” 2020. [Online]. Available: <https://wilselby.com/research/arducopter/controller-design/>. [Accessed May 20, 2025].
- [5] R. Mahony, V. Kumar, and Z. Chen, “Passivity-based control of a quadrotor UAV,” in *2012 IEEE International Conference on Robotics and Automation (ICRA)*, St. Paul, MN, USA, 2012, pp. 1599–1604.
- [6] M. Karahan and C. Kasnakoğlu, “Nonlinear Modeling and Lyapunov Stability Based Controller Design of a Quadrotor UAV,” in *3rd International Informatics and Software Engineering Conference (IISEC)*, 2022, pp. 1–6.
- [7] J. M. A. Costa, M. J. R. Cardoso, and J. A. T. Machado, “Modeling and control of a quadrotor UAV,” *Journal of Vibration and Control*, vol. 20, no. 10, pp. 1548–1560, 2014.
- [8] S. Bouabdallah, “Design and Control of a Quadrotor,” Ph.D. dissertation, École Polytechnique Fédérale de Lausanne, Lausanne, Switzerland, 2007.
- [9] A. T. T. Taha, M. F. R. Khan, and W. W. A. Wahab, “Modelling and Control of a Quadrotor UAV: A Survey,” *International Journal of Automation and Control Engineering*, vol. 3, no. 1, pp. 1–10, 2020.